HHS Public Access

Author manuscript

Cell Rep. Author manuscript; available in PMC 2024 January 03.

Published in final edited form as:

Cell Rep. 2023 October 31; 42(10): 113144. doi:10.1016/j.celrep.2023.113144.

Replication stress and defective checkpoints make fallopian tube epithelial cells putative drivers of high-grade serous ovarian cancer

Pamoda Galhenage[1,7], **Yunlan Zhou**[2,6,7], **Erica Perry**[1], **Brenda Loc**[1], **Kelly Fietz**[1], **Sonia Iyer**[3], **Ferenc Reinhardt**[3], **Tiego Da Silva**[1], **Vladimir Botchkarev**[2], **Jie Chen**[4], **Christopher P. Crum**[5], **Robert A. Weinberg**[3], **Shailja Pathania**[1,8,*]

[1]Center for Personalized Cancer Therapy, Department of Biology, University of Massachusetts Boston, Boston, MA 02125, USA

[2]Dana-Farber Cancer Institute, Boston, MA 02215, USA

[3]Whitehead Institute for Biomedical Research, 455 Main Street, WHTH-367, Cambridge, MA 02142, USA

[4]Department of Mathematics, University of Massachusetts Boston, Boston, MA 02125, USA

[5]Department of Pathology, Division of Women's and Perinatal Pathology, Brigham and Women's Hospital, Boston, MA 02115, USA

[6]Present address: Department of Laboratory Medicine, Xinhua Hospital, Shanghai Jiaotong University School of Medicine, Shanghai 200092, China

[7]These authors contributed equally

[8]Lead contact

SUMMARY

Clinical and molecular evidence indicates that high-grade serous ovarian cancer (HGSOC) primarily originates from the fallopian tube, not the ovarian surface. However, the reasons for this preference remain unclear. Our study highlights significant differences between fallopian tube epithelial (FTE) and ovarian surface epithelial (OSE) cells, providing the molecular basis for FTEs as site of origin of HGSOC. FTEs, unlike OSEs, exhibit heightened replication stress (RS), impaired repair of stalled forks, ineffective G2/M checkpoint, and increased tumorigenicity.

*Correspondence: Shailja.pathania@umb.edu.

AUTHOR CONTRIBUTIONS

S.P. conceived the project and supervised the work. P.G., Y.Z., and S.P. designed the experiments and wrote the manuscript with assistance from R.A.W. Experiments were performed by P.G., Y.Z., E.P., B.L., K.F., and T.D.S. The FACS-based experiments were carried out by V.B. S.I. generated *Pten* KO mouse cells for the mouse tumor studies. F.R. assisted with OFP injections and mouse tumor data analysis under the guidance of R.A.W. C.P.C. provided human ovarian and fallopian tube epithelial tissue from non-*BRCA1*- and *BRCA1*-mutant women. J.C. assisted with the statistical analysis for 53BP1 analysis of human tissue sections. All authors contributed to the writing and editing of the manuscript.

SUPPLEMENTAL INFORMATION

Supplemental information can be found online at https://doi.org/10.1016/j.celrep.2023.113144.

DECLARATION OF INTERESTS

The authors declare no competing interests.

BRCA1 heterozygosity exacerbates these defects, resulting in RS suppression haploinsufficiency and an aggressive tumor phenotype. Examination of human and mouse sections reveals buildup of the RS marker 53BP1 primarily in the fallopian tubes, particularly at the fimbrial ends. Furthermore, menopausal status influences RS levels. Our study provides a mechanistic rationale for FTE as the site of origin for HGSOC, investigates the impact of *BRCA1* heterozygosity, and lays the groundwork for targeting early HGSOC drivers.

In brief

Galhenage et al. elucidate why HGSOC originates from the fallopian tube, not the ovarian surface. They reveal FTE cells' vulnerability to replication stress (RS) and checkpoint defects. Human fallopian tube sections show RS, primarily in the fimbrial ends. Menopause status influences this stress, and Brca1 heterozygosity exacerbates these defects and accelerates tumorigenesis.

Graphical abstract

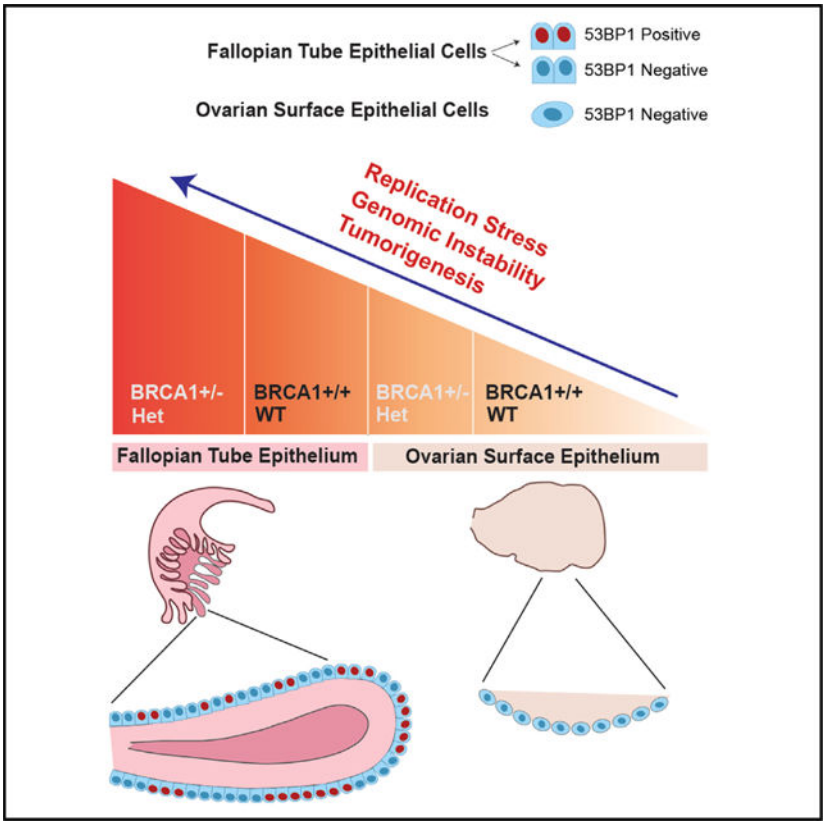

INTRODUCTION

High-grade serous ovarian carcinoma (HGSOC) is the most common subtype among epithelial ovarian cancers (EOC) and accounts for around 60% of all EOCs.[1–3] It is also the deadliest, with the lowest survival rate among all gynecologic malignancies.[3,4] One underlying characteristic of HGSOC is a state of high genomic instability, presumably arising from the loss of function of genes that are associated with DNA damage repair.[5–7]

BRCA1 and *BRCA2* are the most common DNA damage repair genes that are inactivated in HGSOC, through either germline or somatic mutations or promoter hypermethylation.[8,9] Together, loss of function of these genes is associated with ~30% of all HGSOCs.

BRCA1 and BRCA2 are key players in homologous recombination-dependent double-strand break repair (HR DSBR). It is widely accepted that the loss of HR function is one of the driving events in HGSOC.[9–11] Genomic studies have consistently shown defective HR in approximately 50% of HGSOC tumors, further supporting the correlation between HR deficiency and HGSOC.[4,9] While the primary focus has traditionally been on the role of *BRCA1* and *BRCA2* in HR, recent research has revealed their critical involvement in stalled replication fork repair (SFR) and the suppression of replication stress.[12] Chronic replication stress is a well-established driver of epithelial cancer.[13,14] This raises the intriguing possibility that defects in either SFR or HR or both could be early contributors to the pathogenesis of HGSOC, especially in the context of *BRCA1/2* mutant HGSOC.

Previous understanding associated with the cell of origin of HGSOC suggested that the ovarian surface epithelium and/or the ovarian inclusion cysts were the primary precursors of HGSOC. It was proposed that the repetitive damage to the ovarian surface epithelium during each ovulatory cycle could over time drive neoplastic transformation of the ovarian surface epithelial (OSE) cells.[1,15] However, multiple studies have now presented evidence that the fallopian tube epithelium, more specifically, the secretory cells of the fallopian tube, serve as the primary site of origin for HGSOC.[16–18] This hypothesis is supported by the identification of premalignant lesions called serous tubal intraepithelial carcinoma (STIC) in the fallopian tubes of *BRCA1/2* mutation carriers who undergo salpingo-oophorectomy.[19,20] STIC lesions, when present, quite often (~90% of the time) carry a P53 mutation identical to that of the adjacent HGSOC.[21,22] Mouse models and transcriptomic and proteomic profiling of STIC and HGSOC also support the hypothesis that fallopian tube epithelial (FTE) cells serve as the primary site of origin for HGSOC.[23–25] More recently, studies in mouse and organoid-based models have also suggested the possibility of a dual origin of HGSOC whereby both OSE and FTE cells, with appropriate genetic alterations, have the ability to initiate HGSOC.[26,27]

To gain insights into the underlying mechanisms driving the initial stages of HGSOC and determine the susceptibility of fallopian or ovarian cells in its development, we worked with isogenic mouse OSE and FTE cells. Given that defects in DNA damage repair pathways, especially in *BRCA1/2*-mutant HGSOC, play a crucial role in disease progression, we utilized these matched cell pairs to carry out a comprehensive analysis of DNA damage repair defects between OSE and FTE cells. Our study identifies early events that drive genomic instability and provides mechanistic understanding into why FTE cells are more likely to serve as the cell of origin for HGSOC tumors. We also extended our analysis to study the effect of *BRCA1* heterozygosity on DNA damage repair in FTE and OSE cells. We found that *BRCA1* haploinsufficiency for replication stress suppression contributes to increased genomic instability and accelerated tumorigenesis.

Finally, our analysis of human fallopian and ovarian sections sheds light on the varying levels of replication stress in different tissues (ovarian and fallopian) and in different regions of the fallopian tube and the influence of BRCA1 mutations and menopausal status.

Collectively, these findings provide compelling evidence supporting FTE cells as the principal site of origin for HGSOC and highlight replication stress as an early driver of HGSOC.

RESULTS

Isolation and characterization of isogenic mouse ovarian and fallopian epithelial cell lines

We worked with paired isogenic mouse fallopian and ovarian cell lines derived from the fallopian tissue and ovarian tissue, respectively, of the same mouse to compare DNA damage repair efficiency between these two cell types.

We harvested ovarian and oviduct tissue from two mice (M412 and M56; both 14 weeks of age) and derived isogenic pairs of mouse OSE (mOSE) and mouse FTE (mFTE) cell lines. M412 and M56 are genetically deleted for *Trp53* ($p53^{-/-}$) (Figure 1A). These mice have been described previously.[14,28] More specifically, in mouse M412, one allele of the *Trp53* gene is deleted in the germline and the other is flanked by *loxP* sites ($Trp53^{flox/del}$) and deleted through the action of *Meox2-Cre*, which is expressed early during embryogenesis (E5).[29] In mouse M56, both alleles of *Trp53* are deleted in the germline. Genotypes were confirmed by PCR-based genotype analysis (Figures S1A, S1B, and S1C).

The ovarian and fallopian origin of the mOSE and mFTE cell lines, respectively, was confirmed by using the epithelial cell marker CK8[26,30] (Figure 1B) and fallopian markers Pax8 and Sox17, which also confirmed their secretory lineage (Figures 1B and S1D).[16,31] Given that DNA damage repair efficiency can be affected by cell-cycle distribution and proliferation rates, we also confirmed that the cell-cycle profiles and the proliferation rates of mOSE and mFTE lines were similar by using the bromodeoxyuridine (BrdU)-based fluorescence-activated cell sorting (FACS) analysis (Figure S1E).

mFTE cells reveal increased sensitivity to replication-stress-inducing agents compared with their paired mOSE counterparts

We compared the sensitivity of paired mFTE and mOSE lines to different DNA-damaging agents. We evaluated their sensitivity to stalled fork-inducing agents like hydroxyurea (HU) and cisplatin[14,32] and to etoposide that primarily causes double-strand breaks. mFTE cells were more sensitive to the replication-stress-inducing agents (HU and cisplatin) (Figures 1C, 1D, S2A, and S2B) compared with mOSE cells. Interestingly, no such difference in drug sensitivity between mFTE and mOSE was found in response to the double-strand break (DSB)-inducing agent etoposide (Figures 1E and S2C). To further confirm that the efficiency of DSBR was indeed similar in mOSE and mFTE cells, we examined the recruitment of Rad51 to the sites of DSBs induced by ionizing radiation (IR; 10 Gy). The percentages of cells that showed Rad51 focus formation after IR were similar in paired mOSE and mFTE cells (Figures 1F and 1G). Taken together, these findings suggest that, while both mOSE and mFTE cells exhibit a comparable response to DSB-inducing damage, mFTE cells display

greater sensitivity than their isogenic mOSE counterparts when it comes to DNA damage caused by replication stress.

mFTE cells are innately inefficient in replication-stress response

The marked sensitivity of mFTE cells to replication-stress-inducing agents led us to investigate the ability of mFTE and mOSE cells to handle stalled replication forks and their respective responses to replication stress.

To assess the ability of mFTE and mOSE cells to repair stalled replication forks, we analyzed loading of phosphorylated RPA32 (pRPA) on chromatin in cells undergoing replication stress induced by HU. Loading of pRPA on ssDNA at stalled forks serves as a signaling step for launching SFR and checkpoint activation.[33,34] Defective pRPA loading on chromatin after replication stress is one of the indicators of a defective SFR pathway. Indeed, we observed that upon HU-induced replication fork stalling, mFTE cell lines exhibited a deficiency in the accumulation of pRPA (phosphorylated at S4/S8) on chromatin in comparison with mOSE cell lines (Figure 2A). This was true for both the isogenic pairs used in this study (M412 and M56, Figure S2D).

pRPA loading on ssDNA stimulates ATR-dependent CHK1 phosphorylation.[35] Consistent with the reduced accumulation of pRPA at HU-induced stalled forks, we found that Chk1 phosphorylation was also defective in mFTEs in comparison with mOSEs (Figures 2B and S2E). Taken together, these observations provided further evidence in support of a cell-intrinsic inefficiency of fallopian tube-derived cells to suppress replication stress compared with the OSE cells.

We next analyzed the stability of stalled replication forks by performing the DNA fiber assay. HU (5 mM) was added for 3 h to stall replication forks, and nascent fork degradation was measured post-HU treatment (Figure 2C, top). IdU- and CldU-labeled tracts were measured, and any reduction in CldU/IdU ratio served as a measure of fork instability. Figure 2C shows representative images of DNA fibers in mOSE and mFTE cells with and without HU treatment. This analysis revealed a significantly higher degree of stalled fork degradation in mFTE cells compared with their paired isogenic mOSE counterparts. (Figures 2C, 2D, and S2F).

53BP1 is known to associate with chronically stalled and/or collapsed forks.[36,37] In keeping with the increased fork degradation and inefficient SFR pathway response, mFTE cells displayed significantly higher 53BP1 foci formation, indicating fork stalling/collapse compared with mOSE cells (Figures 2E and 2F). This was also confirmed by increased γ-H2AX staining in mFTE cells compared with mOSE cells. Exposure to HU and cisplatin, and the subsequent recovery of the treated cells, revealed that mFTE cells continue accumulating DNA damage (presumably as replication forks continue collapsing) during the recovery phase (Figure 2G).

These results support the hypothesis that FTE cells are prone to increased replication stress compared with cells from the ovarian surface epithelium.

Checkpoint activation is impaired in fallopian tube epithelial cells compared with ovarian surface epithelial cells

CHK1 phosphorylation upon DNA damage is associated with activating the G2/M checkpoint.[38,39] Given that our data revealed inefficient CHK1 phosphorylation in mFTE lines upon replication stress, we tested if the G2/M checkpoint control was also inefficient in the mFTE cells.

To evaluate G2/M checkpoint efficiency, we analyzed the populations of mOSE and mFTE cells that accumulate in G2/M upon treatment with the replication-stress-inducing agent HU. We used phosphorylated (S28) histone H3 (pH3 S28) to mark mitotic cells.[40] mOSE and mFTE cells were treated with HU (2 mM for 5 h) and then released into fresh medium containing nocodazole (Noc) to trap cells entering mitosis. In control cells (no HU and/or Noc), similar percentages of mOSE and mFTE cells pass through mitosis (Figures 3A and 3B). However, after HU-induced DNA damage and in the presence of Noc, the percentage of pH3 (S28)-positive cells was significantly higher in mOSE cells compared with mFTE (Figures 3A and 3B). This suggested to us that, although both mOSE and mFTE cells have similar percentages of cells moving through mitosis under normal conditions, upon replication stress a greater proportion of mFTE cells tend to bypass the G2/M checkpoint.

To further confirm the defect in G2/M checkpoint, we analyzed the percentage of cells that exit G2/M and enter the next G1 phase upon replication stress. An effective G2/M checkpoint should arrest cells in G2/M and not allow them to enter the next G1 phase. We labeled the S-phase cells by pulse labeling with BrdU for 1 h, and then followed them after treatment with HU (5 mM for 5 h; Figures 3C, 3D, and 3E). As expected, 7 h post-BrdU pulse, the G1 populations in untreated mOSE and mFTE cells showed similar percentages of BrdU-positive cells. These cells originated from undamaged cycling cells that were labeled with BrdU during the S phase and had subsequently progressed through G2/M into the subsequent G1 phase (Figures 3D, 3E, and S2G). Interestingly, following treatment with HU and subsequent release for 7 h, a significant proportion of BrdU-positive mFTE cells (indicated as fluorescein isothiocyanate [FITC] positive) continued to cycle through G2/M and entered the next G1 phase, in contrast to mOSE cells (Figures 3D, 3E, and S2G).

Taken together, these data indicate that FTE cells, but not OSE cells, are inherently inefficient in activating the G2/M checkpoint upon replication stress.

Increased micronucleus formation upon replication stress in mFTE cells compared with their mOSE counterparts

A defective G2/M checkpoint allows the cells to enter mitosis even in the presence of unrepaired DNA breaks, thereby resulting in lagging and/or broken chromosome fragments. These broken chromosome fragments often manifest themselves as micronuclei.[41] Therefore, we analyzed the occurrence of micronucleus formation in mFTE and mOSE cells upon replication stress. In this set of experiments, cells were treated with 5 mM HU for 5 h or with 2 μM cisplatin for 5 h. Subsequently, the drugs were removed, and the cells were allowed to recover for 48 and 24 h, respectively, and analyzed for micronucleus formation. The micronucleus analysis revealed elevated levels of micronucleus-positive mFTE cells,

approximately 2-fold higher than those observed in mOSEs (Figures 3F and 3G). This was true for both cisplatin- and HU-treated mFTE cells. A similar increase in micronucleus formation was also observed for mFTE cells from the second isogenic pair (M56) (Figures S2H and S2I).

We also carried out micronucleus analysis for three additional sets of mFTEs vs. mOSEs derived from wild-type P53 mice. As mentioned above, M412- and M56-derived mOSEs and mFTEs are deleted for p53. Loss of p53 could potentially influence the DNA damage repair characteristics of FTEs and OSEs. Hence, we investigated whether mOSEs and mFTEs with intact p53 also displayed the same DNA damage repair profiles as cells lacking p53. As illustrated in Figures S2J and S2K, similar to the M412 and M56 sets, the p53 wild-type mFTE cells exhibited a higher propensity for micronucleus formation compared with the p53 wild-type mOSE cells. These findings indicate that the inability of FTE cells to repair DNA compared with OSE cells is not influenced by the P53 status.

BRCA1 heterozygous mOSEs and mFTEs are haploinsufficient for replication-stress suppression

BRCA1 heterozygous skin fibroblasts and mammary epithelial cells have been shown previously to be haploinsufficient for stalled fork repair and replication-stress suppression.[14,32] Such haploinsufficiency for replication-stress suppression is considered one of the early steps toward tumorigenesis.[14,32] Thus, we wondered whether *BRCA1* heterozygous OSE and FTE cells were similarly compromised in their ability to carry out SFR and were, as a direct consequence, at increased risk of replication stress, genomic instability, and tumorigenesis.

We generated mOSE and mFTE cell lines from two *Brca1* heterozygous ($Brca1^{wt/del}$) mice (M338 and M4). Like the *Brca1* WT lines, $Brca1^{wt/del}$ M338 and M4 were also deleted homozygously for *p53*. We confirmed the deletion of the *Brca1* and *Trp53* alleles by carrying out PCR-based genotyping assay (Figures S1A, S1B, and S1C). The proliferation profiles of *Brca1* heterozygous M338 and M4 mOSE and mFTE cell lines were similar to those of *Brca1* wild-type (WT) mOSE and mFTE lines (Figure S3A). Like M412 and M56 FTEs, the M338 and M4 mFTE lines were also confirmed to be derived from FTE tissue by Pax8 immunostaining (Figure S3B). In addition, their epithelial origin was confirmed by positive CK8 immunostaining (Figure S3B).

To determine whether *Brca1* heterozygosity further sensitizes mOSE and mFTE cells to replication-stress-inducing agents, we assessed cell survival after HU and cisplatin treatments. Our data reveal that both *Brca1* heterozygous mOSE and mFTE lines were more sensitive to HU and cisplatin compared with the *Brca1* WT counterparts (Figures 4A and 4B). Given that *Brca1* WT mFTE cells are already sensitive to HU and cisplatin, an additional increase in sensitivity in *Brca1* heterozygous mFTE cells was difficult to detect.

pRPA accumulation on chromatin upon HU-induced replication stress is also affected in *Brca1* heterozygous mOSE and mFTE cells compared with their WT counterparts (Figures 4C and 4D). Furthermore, DNA fiber assays revealed increased fork degradation in *Brca1* heterozygous mOSE and mFTE cells compared with *Brca1* WT cells (Figure 4E). In

keeping with defective SFR in *Brca1* heterozygous cells, these cells also showed a higher percentage of cells with 53BP1 foci than *Brca1* WT cells (Figures 4F and 4G). Similar experiments were also carried out with the second pair of Brca1 heterozygous mOSE and mFTE lines (M4). Here too, Brca1 heterozygosity resulted in increased sensitivity to the replication stalling agent cisplatin, reduced pRPA (S33) loading after HU, and increased micronucleus formation after cisplatin and HU (Figures S3C, S3D, and S3E). These data further confirm that *Brca1* heterozygous mOSE and mFTE cells are haploinsufficient for stalled fork repair.

FTE cells are more tumorigenic than OSEs, and *BRCA1* heterozygosity accelerates tumorigenesis

We compared the tumor-forming ability of fallopian and ovarian epithelial cells. Considering haploinsufficiency for replication-stress suppression in *BRCA1* heterozygous cells in our study, we also addressed the effect of *Brca1* heterozygosity on tumor formation. To enable tumor formation, the mOSE and mFTE cells were deleted for *Pten* via CRISPR-Cas9-mediated gene editing. *Pten* mutations are commonly present in *BRCA1* mutant ovarian tumors.[42]

Cells were either subcutaneously injectedinto immune-compromised NSG mice or injected into the ovarian fat pad (OFP) of these mice. Both these approaches revealed that the fallopian tube-derived mFTE cells have higher tumorigenic potential than the ovarian surface-derived mOSE cells (Figures 5A and 5C). In both tumor models mFTE cells formed tumors faster and with significantly higher tumor weight compared with their isogenic ovarian counterparts. Furthermore, in the subcutaneous tumor model, *Brca1* heterozygosity accelerated the tumorigenic potential of both ovarian and fallopian cells (Figures 5A and 5B). Interestingly, in the OFP tumor model, although *Brca1* heterozygosity resulted in accelerated tumorigenesis with higher tumor weight in the mOSE arm, in the mFTE arm, *Brca1* heterozygosity resulted in increased metastasis but not necessarily bigger tumors (Figures 5C, 5D, and 5F). The *Brca1* heterozygous mFTE-derived tumors mostly metastasized to the lungs in this tumor model (Figure 5F). Such lung metastasis has been observed previously in other more aggressive ovarian tumor mouse models.[43–45]

All the tumors showed positive stain for HGSOC-specific markers p16 and Pax8 (Figure 5E). This was also true for the metastasized $Brca1^{+/-}$ mFTE tumors in the lung (Figure 5F). These tumors (BTP mOSE and TP and BTP mFTE) were also positive for the replication stress marker 53BP1 (Figure 5G). This finding is consistent with our observation that FTE cells are prone to increased replication stress and that *Brca1* heterozygosity results in haploinsufficiency for replication stress suppression. Collectively, these analyses confirm that FTE cells possess a higher tumorigenic potential than the OSE cells and that *Brca1* heterozygosity further amplifies the tumorigenic potential of these cells.

Human fallopian tube epithelial cells are susceptible to increased replication stress compared with human ovarian surface epithelial cells

The work described above successfully demonstrated inherent defects in replication-stress suppression and impaired activation of cell-cycle checkpoints in mouse fallopian tube-

derived cells, compared with their isogenic counterparts derived from ovarian surface epithelium. In light of these findings, we sought to investigate whether similar DNA damage repair disparities exist between human fallopian and ovarian epithelial cells. It is important to note that the human fallopian and ovarian epithelial cells we worked with are not isogenic and do not share an identical genetic background. Nonetheless, we pursued this inquiry to explore potential similarities or differences in DNA damage repair mechanisms in human counterparts.

The questions here remained the same: whether FTE cells exhibit compromised DNA damage repair capabilities and impaired checkpoint activation compared with OSE cells. To address these questions, we worked with two immortalized human OSE (HOSE) lines, IHOSE1431 and HOSE, and two human FTE (HFTE) lines, HFTE237 and HFTE194 (Figure 6A), which have been previously described.[30,46–48] These cell lines were isolated from healthy human ovaries and fallopian tubes from patients without cancer. We confirmed the epithelial cell origin for all the lines by using the epithelial cell marker CK8 and the fallopian tube origin for the HFTE cell lines by staining for PAX8[26,49] (Figure S4A). In addition, FACS-based analysis of BrdU incorporation into the cells confirmed that HOSE and HFTE lines had similar cell-cycle profiles and proliferation rates (Figure S4B).

Consistent with our findings in the mouse cells, we found that human FTE cells (HFTE237 and HFTE194) exhibited a significant reduction in accumulation of pRPA (S33) on chromatin compared with HOSE lines (IHOSE1431 and HOSE) following treatment with HU (Figure 6B). In addition, HFTE cells displayed reduced CHK1 phosphorylation compared with HOSE cells upon replication stress (Figure 6C).

We nextanalyzed the efficiency of G2/Mcheckpoint activation in HOSE and HFTE cells. Here too, both HFTE lines showed a reduction in the percentage of cells undergoing arrest in mitosis after treatment with HU relative to the human ovarian lines (Figures 6D and 6E). This agrees with checkpointdata from the mouse cell lines presented above. Together, this reveals that FTE cells are indeed inefficient in mounting a robust stalled fork repair response and are defective in G2/M cell-cycle checkpoint activation.

To address the potential impact of p53 loss on the replication-stress suppression ability of FTE cells, we directly compared P53 WT HOSE and HFTE lines. Specifically, we worked with IHOSE1431 and HFTE194, because both these lines are WT for P53 (Figure S4C). Specifically, we selected IHOSE1431 and HFTE194 cell lines due to their WT P53 status. However, IHOSE1431 lacks htert gene expression, unlike HFTE194. To ensure genetic similarity, we introduced htert into IHOSE1431 cells (IHOSE1431ht), thereby creating a comparable set of modified cell lines. When we compared these lines, we observed that FTE line HFTE194 was defective in RPA loading after HU-induced replication stress, defective in activation of G2/M checkpoint, and more prone to micronucleus formation (Figures S4C, S4D, S4E, and S4F) upon DNA damage. These findings provide further evidence that FTE cells, irrespective of their p53 status, are compromised in their ability to suppress replication stress compared with OSE cells.

Cells in fallopian tube sections reveal increased replication stress compared with the ovarian surface sections

Having established that the FTE cells are innately prone to high replication stress compared with OSE cells, we next asked whether we could find evidence of this phenomenon in the mouse and human tissue sections. Specifically, we sought to examine paired ovarian and fallopian sections derived from the same mice and from the same individuals to determine whether the FTE sections show evidence of increased replication stress in comparison with the OSE sections. We used 53BP1, a known replication stress marker,[14,50] to address this question. Paired fallopian tube and ovarian surface sections from three mice (1427, 1638, and 569) and paired fallopian and ovarian sections from six different individuals were stained with 53BP1. Among these individuals, three were WT for *BRCA1* (A1, A2, and A3) and three were heterozygous for *BRCA1* (B1, B4, and B5). Our data consistently demonstrate that, for all the cases (three mice and six individuals), the FTE sections show evidence of replication stress, while the OSE sections do not (Figures 7A, 7B, S5A, and S5B). We also tested whether a certain fallopian cell type, i.e., secretory and/or ciliated, is more prone to accumulating 53BP1 signal. Pax8 antibody was used to mark the secretory cells. As shown in Figure S5D, in mouse fallopian tube sections, both ciliated and secretory cells are similarly susceptible to increased replication stress. This is evident by the observation that both Pax8-positive and Pax8-negative cells stain with 53BP1 antibody. We used FOXJ1 antibody, which stains ciliated cells, to address the nature of cells that stain positive for 53BP1 in human sections. Here, too, we found that both ciliated (FOXJ1 positive) and secretory (FOXJ1 negative) cells stain with 53BP1 (Figure S5E).

Ki67 staining was used to determine the proliferation status of the ovarian and the fallopian sections. Our data indicate that the difference in replication stress signal between these two tissue types is not related to their proliferation status (Figure S5F). It remains to be determined whether *BRCA1* heterozygosity contributes toward additional replication stress in the fallopian sections. The evidence presented in this study does suggest an increased percentage of 53BP1-positive cells in the fallopian tube from *BRCA1* mutation carriers (Figure 7B), but due to limited sample size, the data do not reach statistical significance. Nevertheless, the analysis of paired mouse and human fallopian and ovarian sections provides unequivocal evidence that FTE cells experience increased replication stress compared with their ovarian surface counterparts.

Fimbrial ends of the fallopian tube are more prone to replication stress than the proximal ends, and the effect of menopausal status on replication stress

Fimbrial ends, which are in close proximity to the ovary, harbor precancerous lesions that could potentially give rise to HGSOC. In addition, the fimbrial ends could be particularly susceptible to replication stress due to their exposure to reactive oxygen species (ROS) through the follicular fluid released during ovulation.[51,52] Taking these factors into consideration, we wondered whether the fimbrial ends of the fallopian tube exhibit heightened replication stress compared with the proximal ends. To address this, we conducted a comparative analysis of replication stress levels between the proximal region (including the isthmus and ampulla closer to the uterus) and the distal region (fimbrial ends) of the same women.

Despite the limited sample size, we consistently saw that the isthmus/ampulla region of the fallopian tube shows significantly lower 53BP1 signal compared with the fimbrial region (Figures 7C and 7D). Interestingly, we detected increased 53BP1 levels in the isthmus/ampulla region of *BRCA1* mutant cases compared with *BRCA1* WT cases (Figure S5C). Together our results suggest that the distal end of the fallopian tube, specifically, the fimbrial end, exhibits higher 53BP1 staining than the proximal end.

Given the connection between ovulation and ovarian cancer[53–55] and considering the previously discussed evidence of increased replication stress in the fimbrial ends (Figures 7A and 7B), we next focused on exploring the possible correlation between menopausal status and 53BP1 staining levels in the fallopian tubes. To conduct this analysis, we performed 53BP1 staining on sections of the fimbrial ends obtained from premenopausal (pre-M) and post-menopausal (post-M) women, both with and without *BRCA1* mutations (Figure 7E). For each group, we examined three individual cases. We found significant increase in 53BP1 staining in the fimbrial sections from pre-M women compared with post-M women without *BRCA1* mutation (Figure 7F). However, this difference between pre- and post-menopausal tissue sections was not observed in sections from women with the *BRCA1* mutation, mainly due to persistence of 53BP1 staining in post-menopausal fimbrial tissue from *BRCA1* mutation carriers (Figure 7F). It is important to note that we were unable to gather information on the ovulation cycles of the pre-M women in this study, limiting our ability to assess the potential impact of ovulation on these sections.

Together, these findings indicate that fimbrial ends undergo increased replication stress compared with the proximal ends of the fallopian tube and that menopausal status can potentially affect the extent of replication stress in the fimbrial end based on the *BRCA1* mutation status.

DISCUSSION

Investigating the cell of origin for cancer is a crucial undertaking that not only enhances our understanding of disease etiology but also directs our attention toward specific cell types to identify early events that promote tumor development. By understanding the origins of cancer at the cellular level, we can gain valuable insights into the disease and its underlying mechanisms. For HGSOC, the current understanding, based on mouse models,[30,56] transcriptomic and proteomic profiling,[24,57,58] and work with FTE and OSE organoids,[26,27] is that FTEs are most likely the cells of origin.

In this study we provide the mechanistic basis for why FTEs might be more tumorigenic compared with OSEs, establishing their role in driving ovarian cancer. Our findings provide evidence that FTE cells are particularly compromised in their ability to repair stalled replication forks, suppress replication stress, and activate the G2/M checkpoint. We also show that *BRCA1* heterozygosity amplifies replication stress in FTEs, rendering them more tumorigenic. Furthermore, our work with human fallopian and ovarian sections obtained from women with and without *BRCA1* mutations reveals a striking accumulation of 53BP1, a marker for replication stress and DNA damage, predominantly at the fimbrial ends of the fallopian tube. In contrast, the proximal ends of the fallopian tubes display minimal 53BP1

staining, and the ovarian surface epithelium even less so. We go on to investigate the effect of menopausal status on the accumulation of 53BP1 at the fimbrial ends.

Collectively, based on findings presented in this study, we propose that FTE cells, especially those in the fimbrial ends, are at an increased risk of accumulating genomic instability. Consequently, these cells emerge as the primary cell of origin for the initiation of ovarian tumorigenesis.

Despite the strong linkage between defective HR DSBR and HGSOC,[9,59,60] we find no apparent defect in HR DSBR in either FTE or OSE. However, in contrast to the normal HR DSBR in FTEs and OSEs, SFR and replication-stress suppression are ineffective in FTEs compared with the isogenic OSE counterparts. This raises the interesting possibility that, despite the historical emphasis on HR defects as a primary driver of HGSOC, it is actually the defective stalled fork repair and the accumulation of replication stress that play an early role in the development of HGSOC. This hypothesis aligns with the well-established association between defective SFR and the onset of epithelial cancers.[14,61,62] Increased replication stress has also been linked to ovarian cancer, and recent studies have looked for ways to target this through new therapeutic strategies for ovarian cancer.[63–65] The compromised ability of FTEs to effectively handle stalled replication forks and consequently accumulate DNA damage upon replication stress renders them acutely vulnerable to genomic instability. We propose that this susceptibility positions FTEs as significant contributors to the initiation and progression of ovarian cancer.

A key step in suppressing tumorigenesis is effective checkpoint activation after DNA damage. In this study we find that FTEs are especially compromised in activating the G2/M checkpoint and tend to show a high incidence of micronucleus formation compared with their isogenic OSE counterparts. We propose that such checkpoint defects exist early in the FTE cells, and its dysregulation, presumably by modulation of checkpoint genes, could eventually provide the FTE cells with the survival advantage that could lead to tumorigenesis.

Germline heterozygous *BRCA1* mutations predispose women to high risk for HGSOC,[7,8,25] and *BRCA1* haploinsufficiency, especially for replication-stress suppression, has been shown previously.[14,32] In our study, OSEs and FTEs derived from *Brca1* heterozygous mice ($Brca1^{wt/del}$; $Trp53^{del/del}$) reveal that these cells undergo increased replication stress and genomic instability compared with the OSEs and FTEs from *Brca1* WT mice ($Brca1^{wt/wt}$; $Trp53^{del/del}$). Such innate SFR defect in *BRCA1* heterozygous cells could, in principle, represent the first in a chain of events that occur in *BRCA1* heterozygous fallopian and ovarian epithelial cells on their way to ovarian cancer development.

Our tumor study reveals that, although both OSEs and FTEs can induce tumorigenesis when injected subcutaneously or into the OFP in immunodeficient mice, it is the FTEs that are more prone to tumorigenesis. Furthermore, *Brca1* heterozygosity increased the tumorigenic potential of both OSEs and FTEs and resulted in faster tumor growth. This suggests that, even though *BRCA1* haploinsufficiency for replication-stress suppression could drive tumorigenesis from ovarian surface epithelium, the *BRCA1* heterozygous fallopian tube

cells within the same individual remain more defective in DNA damage repair and are more predisposed to tumorigenesis than their ovarian counterparts.

In the case where cells were injected into the OFP, it is interesting to note that *BRCA1* heterozygosity in FTE cells induced metastasis. There is not much evidence for increased metastasis except for some cases of increased brain metastasis[66,67] in ovarian cancer. We suspect the increased evidence of lung metastasis that we see in our study reflects the more aggressive nature of FTE-derived *BRCA1*-mutant ovarian cancer.

The data from our mouse and human section analysis suggest several significant findings. First, our data demonstrate that the FTE cells are more susceptible to replication stress, as evidenced by positive 53BP1 staining, compared with OSE cells. Both ciliated and secretory cells of the fallopian tube show 53BP1 staining. How the distribution of 53BP1-positive ciliated and secretory cells changes based on the location of these cells within the fallopian tube, i.e., distal or proximal ends, and/or other factors, such as menopause, age, parity, *BRCA1/2* status, etc., remains to be seen.

In our study, examination of different sections of the fallopian tube revealed that the fimbrial ends of the fallopian tube experience higher levels of replication stress compared with the proximal ends, such as isthmus and ampulla. This finding supports the hypothesis that fimbrial ends, located in close proximity to the ovarian surface, may be exposed to ROS during ovulation, rendering them more prone to replication stress.[51,52,68] Interestingly, despite being the site of ovulation, we find that the ovarian surface does not display signs of replication stress. Our data suggest that this may be attributed to the superior ability of OSE cells to suppress replication stress compared with FTE cells.

When comparing the presence of 53BP1-positive cells in *BRCA1* WT vs. *BRCA1* mutant distal/fimbrial ends, we observed a trend for higher percentage of 53BP1-positive cells in *BRCA1* mutant fimbrial ends. Although our sample size was small, it does suggest that *BRCA1* haploinsufficiency may contribute to the accumulation of replication stress in FTEs. This is in keeping with our cell-line-based experiments. The higher 53BP1 staining in *BRCA1* heterozygous cells also supports a previous report that identified elevated 53BP1 protein expression in *BRCA1*-mutant ovarian carcinomas.[69]

Finally, our data indicate a potential correlation between menopausal status and the extent of replication stress in the fimbrial end, particularly in relation to the presence of *BRCA1* mutations. Specifically, pre-M women exhibited increased 53BP1 staining in the fimbriae sections compared with post-M women without *BRCA1* mutations. However, this difference was not observed in women with *BRCA1* mutations, as post-M fimbriae tissue in these cases retained strong 53BP1 staining. It remains to be seen whether *BRCA1* mutation in post-M women renders their fallopian tissue susceptible to chronic replication stress. It is important to note that further investigation is needed to assess the effect of ovulation on the observed results, which could not be assessed due to the lack of available information on the ovulation cycles of the pre-M women included in the study.

This study has important implications not only for the evolution of HGSOC but also for the design of therapeutic strategies for HGSOC. The weaknesses identified in our study in FTE

cells, i.e., increased replication stress and defective G2/M checkpoint, provide avenues for future therapeutic strategies.

Limitations of the study

One limitation of our study is that the isogenic mouse lines we worked with lack P53. We encountered difficulties in deriving stable P53-WT lines from the fallopian and ovarian tissue of the p53-WT mice. This limited our ability to conduct comprehensive analysis on isogenic fallopian and ovarian cell lines with intact p53. It remains plausible that the loss of p53, which is a common occurrence in HGSOC, may have a varying impact on either the fallopian or the ovarian cell type. Nevertheless, the micronucleus analysis that we were able to carry out on short-term cultures of p53-WT FTEs and OSEs (using three different lines) after treatment with cisplatin or HU does suggest that p53 status might not significantly influence the increased sensitivity to replication stress observed in FTE cells compared with OSE cells. Both p53-WT and p53-deleted FTE cells were more prone to micronucleus formation compared with their OSE counterparts. Having said that, it will be important to conduct a more extensive analysis with p53-WT lines (if they can be cultured) to investigate whether the presence of p53 selectively affects FTEs more than OSEs, or vice versa.

STAR★METHODS

RESOURCE AVAILABILITY

Lead contact—Further inquiries regarding methods, reagents, or results should be directed to the lead contact, Shailja Pathania (Shailja.Pathania@umb.edu).

Materials availability—This study did not generate unique materials and reagents.

Data and code availability

- Original data are available from the lead contact upon request.
- This paper does not report original code.
- Any additional information required to reanalyze the data reported in this paper is available from the lead contact upon request.

EXPERIMENTAL MODEL AND STUDY PARTICIPANT DETAILS

Human experimental sections—Human ovarian surface epithelial (OSE) and fallopian tube epithelial (FTE) *BRCA1* wildtype (n=7) and mutant unstained tissue (n=7) from pre-menopausal (Pre-M) and post-menopausal (post-M) women were obtained from the Brigham and Women's Hospital pathology [DF/HCC] core. Menopausal status of each case is available through table in Figure 7E. Immunofluorescence based analysis and immunohistochemistry was performed using these sections.

Mouse experimental models—Genetically engineered mouse models were generated by crossing mice harboring the conditional *Brca1*$^{flox/flox}$ Trp53$^{flox/flox}$ allele (kindly provided by Jos Jonker's group)[71] with Meox2-Cre mice obtained from Jackson Labs (Stock

#003755).[29] 14-weeks old female mice were used in this study to generate mOSE and mFTE M412, M56, M338, M4 cell lines.

Animal tumor models were carried out in 6-weeks old NSG (NOD.Cg-*Prkdc*^{scid} *Il2rg*^{tm1Wjl}/SzJ) female mice. All animal experiments in this study were performed according to the guidelines established by the IACUC (Institutional Animal Care and Use Committee) of University of Massachusetts Boston, Dana Farber Cancer Institute, and Massachusetts Institute of Technology.

METHOD DETAILS

Genotyping—The conditional inactivation of *Brca1* and *Trp53* is driven by Cre-mediated recombination of loxp sites flanking *Brca1* exons 5–13 and *Trp*53 exons 2–10 respectively. Mouse genotyping was performed on genomic DNA extracted from mouse tail snips as described previously.[32] 14-week-old *Brca1*$^{wt/wt}$; *Trp53*$^{flox/del}$; Meox2$^{wt/Cre}$ (M412), *Brca1*$^{wt/flox}$; *Trp53*$^{del/del}$; Meox2$^{wt/wt}$ (A56), and *Brca1*$^{wt/del}$; *Trp53*$^{flox/del}$ Meox2$^{wt/Cre}$ (M338 and M4) mice were used in this study. Below are PCR primers used to carry out genotyping.

Meox2Cre wt: CGCGATTATGCAAGACGAGGAAGATGTGGAGAGTTCGGGGTAG

Meox2Cre KI: CTTCTTCTTGGGTCCTCCCAGATCCTCCTCAGAAATCAGC

Meox2Cre common: CCTGAAAGCAGTTCTCTGGGACCACCTTCTTTTGGCTTC

Brca1-A: GGTACCAGTTATGAGTTAGTCGTGTGCCTGAGTCA

Brca1-B: GCTGAGATTAAAGTGCAGGCCACCACACTCAGTGAT

Brca1-C: GCTGTGACATATTCTTACTTCGTGGCACATCTCTCA

Tp53int1F:
ACAAAAAACAGGTTAAACCCAGCTTGACCAAGTGCCATTGGTCCATGGAT

Tp53int1R: AGCACATAGGAGGCAGAGACAGTTGGAGGCCAGCCTGGTCTACAGA

Tp53int10R:GGGGAGGGATGAAGTGATGGGAGCTAGCAGTTTGGGCTTTCCTCCTT
GATCA. All animal experiments in this study were performed according to the guidelines established by Animal Care and Use Committee of Dana Farber Cancer Institute and University of Massachusetts Boston.

Isolation and culture of primary isogenic mouse ovarian surface epithelial cells (mOSE) and mouse fallopian tube epithelial (mFTE) cells—The ovaries and oviducts from 14-week-old genetically engineered mice were collected and separated under microscope. Tissues were triple washed with PBS, dissected with a scalpel and then incubated in 0.25% Trypsin in a 15 ml Falcon tube at 37°C for 30 mins as described previously.[72–74] Trypsin inhibitor was added to terminate digestion. Cells were then centrifuged and resuspended in the growing medium[75] containing DMEM, 4% heat-inactivated fetal bovine serum, 100U/ml penicillin/100μg/ml streptomycin solution

(Sigma-Aldrich), 0.1μg/ml gentamicin (Gibco-R01510), 1μg/ml insulin–transferrin–sodium–selenite supplement (Sigma-Aldrich; 11074547001), and 2 ng/ml recombinant EGF (Gibco; PHG0311L). Primary cells were maintained in tissue culture plates in this media and passaged upon reaching confluence.

Human ovarian and fallopian tube epithelial cell culture—Immortalized human fallopian tube cells (HFTE237 and HFTE194) were provided by Dr. Ronny Drapkin (UPenn, Perelman School of Medicine Philadelphia) and Dr. Robert Weinberg (Whitehead Institute for Biomedical Research, MIT). HFTE cells were cultured in 10% FBS, 1% Pen-strep, and DMEM/Ham's F-12 50/50 (Corning; 15090-CV). Human ovarian surface epithelia cells (HOSE) were provided by Dr. Frances Balkwill (Queen Mary University of London) and cells were cultured in Medium199 (Gibco; 11150–059) and MCDB105 (Sigma Aldrich; 117–500) in 1:1 ratio, and supplemented with 15% FBS, 34μg/ml of Bovine pituitary extract (Life Technologies; 13028014), 0.5μg/ml of Hydrocortisone (Sigma; H0888–1G),[76] 5μg/ml of Insulin human recombinant zinc solution (Life Technologies; 12585014), and 10ng/ml of recombinant human EGF (Gibco; PHG0311L). The second ovarian epithelial IHOSE1431 cell line was provided by Dr. Jae Hoon Kim at Gangnam Severance Hospital Yonsei University of Medicine, Seoul, Republic of Korea. IHOSE1431 cells were cultured in 10% FBS, 1% Pen-Strep, and DMEM.

Immunofluorescence for cell lines—Cells grown on glass coverslips were washed with PBS and fixed with 4% paraformaldehyde/2% sucrose for 10 min at room temperature (RT). Cells on coverslips were washed with PBS and permeabilized with 0.5% Triton X-100 for 4 min at RT. Cells were incubated with respective antibodies for 35 min at 37°C followed by incubation with secondary antibodies (FITC and/or Rhodamine conjugated) for 25 min at 37°C. Finally, coverslips were mounted with 4,6-diamidino-2-phenylindole (DAPI). Primary antibodies used were γH2AX (Millipore; 05–636; 1:5,000), PAX8 (Proteintech; 10336; 1:1000), CK8 (TROMA-I -DSHB; AB_531826; 1:75), 53BP1 (Bethyl Labs; A300–272A; 1:2,000), and Rad51 (Santa Cruz; SC-8349; 1:150). Images were captured using an Axio Imager M2 (Carl Zeiss) equipped with an Axiocam 506 color camera.

Immunoblotting and antibodies—Nuclear extracts were prepared by first lysing the cells in pre-extraction buffer (PEB) (0.5% Triton X-100, 20mM HEPES pH 7,100mM NaCl, 3mM $MgCl_2$, 300mM sucrose in dH_2O). Cells were incubated on ice for 20min in PEB buffer and then centrifuged at 5000 rpm for 10 min. The supernatant represented the cytoplasmic extract. The nuclear pellet was washed with PBS and lysed in high salt buffer NETN400 (400mM NaCl, 20mM Tris-HCL pH 7.8, 0.5% NP-40, 1mM EDTA, and dH_2O) by constant shaking for 1hr at 4°C. The extract was centrifuged at 15000 rpm and the supernatant collected after centrifugation represented the nuclear extract. All buffers were supplemented with protease and phosphatase inhibitors. Antibodies and their dilutions used for western blotting were pRPA32 (S4/S8) (Bethyl Labs; A300–245A; 1:2500), pRPA32 (S33) (Bethyl Labs; A300–246A; 1:2500), Pax8 (Proteintech; 10336; 1:2500), γH2AX (Millipore; 05–636; 1:2500), pCHK1 (Cell signaling; 2348S; 1:1000), CHK1 (Cell signaling; 2360S; 1:1000), Lamin B1 (Cell Signaling; 12586; 1:3000), GAPDH (Santa Cruz; SC-25778; 1:4000), and mouse Brca1 (kindly gifted by Dr. David Livingston).

Immunofluorescence and immunohistochemistry for tissue sections—For both immunofluorescence and immunohistochemistry, FFP embedded tissue sections were deparaffinized in xylene and rehydrated by serial dilution in ethanol and water. Antigen retrieval was performed by heating the slides in 1X citrate buffer pH 6 (Millipore-Sigma, C9999) for 12min under high pressure followed by cooling down for 30 min at RT. Then sections were washed once with PBS for 5min. For immunofluorescence, sections were blocked with 1% bovine serum albumin [BSA], 10% normal goat serum, and 0.3% Triton X-100 for 1.5hr and then incubated with 53BP1 (Bethyl Laboratories; A300–272A; 1:200), or FoxJ1 (Millipore Sigma; HPA005714; 1:200), or 53BP1 (BioLegend; 933002; 1:50), or Pax8 (Proteintech; 10336; 1:600) primary antibodies diluted in 1% BSA, 1% normal goat serum, and 0.3% Triton X-100 for overnight at 4 °C. Finally, sections were incubated with secondary antibody (Alexa Fluor 647) for 1hr at room temperature and then counterstained with DAPI.

For immunohistochemistry, Endogenous peroxidase was quenched using peroxidase block for 35 min and the slides were washed twice with PBS for 5 min, followed by protein block for 2hrs in the humidity chamber after antigen retrieval. Sections were washed twice with PBS and incubated with primary antibodies overnight at 4°C. Then the slides were washed with PBS twice for 5min and Novolink polymer detection kit (Leica; RE71401-CE) was used to carry out the following steps. Incubate the slides with Novolink polymer for 30min followed by PBS washes. Peroxidase activity was developed by using 1:20 dilution of DAB working solution for 7min. Once the slides were rinsed with water, they were counterstained with Harris modified hematoxylin (Fisher Scientific, SH26–500D) for 15min. Finally, the slides were rinsed with water, dehydrated, and mounted with vectashield antifade mounting media (Vector Laboratories; H-1000). Images were acquired with an Axio Imager. M2. Pax8 (Proteintech, 10336; 1:2000), P16 (Santa Cruz, sc-1661; 1:500), and Ki67 (Novusbio, NB500–170) antibody was used to stain the sections.

Cell viability assay—Cell viability was assessed by plating 1500 cells per well in a 96 well plate. 24hrs after plating, cells were treated with either HU, cisplatin, or etoposide for the indicated doses and time. CellTitter-Glo reagent (Promega; G7572) and DMEM was added in a 1:1 ratio to each well, and the assay was carried out based on manufacturer's instructions. Luminescence was quantified using a BMG Lab-tech luminometer.

DNA fiber assay—Cells were first labeled with 25μM IdU analog for 35 min, washed three times with PBS followed by incubation with 300μM CldU analog for 35 min. Cells were washed and treated with HU (5mM) for 3 hrs. Pre-labeled cells were mixed with unlabeled cells at 1:2 ratio, lysed, and spread onto positively coated microscope slides to obtain single DNA fiber tracts. Slides were fixed with methanol/acetic acid (3:1) for 20 min. After denaturation and blocking (2%BSA/PBS), DNA fibers were stained with rat anti-CldU (Abcam; ab6326; 1:400) and mouse anti-IdU (BD Biosciences; 555627; 1:400) for 2 hrs followed by secondary antibody Alexa Fluor 555 goat anti-rat (Invitrogen; A21434; 1:400) and Alexa Fluor 488 goat anti-mouse (Invitrogen; A10684; 1:400) for 1 hr. DNA fibers were visualized through a fluorescent microscope and ImageJ software was used for evaluation of the tract lengths.

Flow cytometry-based cell cycle analysis—Cell cycle analysis was conducted by using FACS. Both human and mouse ovarian and fallopian tube cells were incubated with bromodeoxyuridine (BrdU) for 1hr and then fixed with 70% ethanol overnight. Fixed cells were centrifuged, washed with PBS, and incubated with 1ml of 2M HCL in 0.5% triton X-100/PBS for 30min at RT. Cell pellets were resuspended in PBST (0.05% Tween20 in PBS) and centrifuged at 1500 rpm for 8 min. Supernatant was discarded and the cells were incubated with 0.1M NaBorate (pH 8.5) for 25min. Cells were centrifuged again and labeled with FITC conjugated mouse anti-BrdU (1:10 dilution, BD Pharmingen; 556028) in super blocking buffer (Invitrogen; 37545) for 1hr in the dark at RT. Cells were washed with 4ml of PBST and centrifuged at 1500 rpm for 10 min. Finally, stained cells were resuspended in 300μl of PI/RNAse solution (BD Pharmingen; 550825) and analyzed by flow cytometry.

Cell cycle checkpoint—pH3 (S28) FACS-based analysis was carried out for cells treated with 2mM HU for 5hrs and then 0.1μg/ml of Nocodazole for 18 hrs. Cells were collected and fixed with 70% ethanol at 4°C overnight. Cells were washed with PBS and centrifuged at 1500 rpm for 8min. The pellet was resuspended in 1ml of 0.25% Triton X-100 in PBS and incubated on ice for 15min. After incubation, 2ml of 1% BSA/PBS was added and the cells were centrifuged for 8 min at 1500 rpm. Supernatant was discarded, cells were stained with Alexa Fluor 647 conjugated anti-pH3(S28) (BD Phosflow; 558217; 1:25 dilution) for 3 hrs. Cells were washed with 1% BSA/PBS and resuspended in 300μl of PI for 10 minutes before FACS analysis. G2/M checkpoint was evaluated by first incubating the cells with BrdU for 1hr. After washing off the BrdU, cells were treated with 5mM HU for 5hrs. Cells were collected at indicated time points and fixed in 70% ethanol overnight at 4°C. BrdU staining was carried out as mentioned in the BrdU FACS- based cell cycle analysis.

Micronuclei analysis—mOSE and mFTE lines were seeded onto coverslips and treated with HU (5mM for 5hrs) or cisplatin (2μM for 5hrs). Cells were allowed to recover for 24hrs post cisplatin and 48hrs post HU treatment. Cells were fixed with 4% paraformaldehyde/2% sucrose for 10 min at RT and washed with PBS. Cells were permeabilized with 0.5% Triton X-100 for 4 min at RT and were mounted with DAPI. Percentage of cells with micronuclei were examined (3 or more micronuclei per nuclei was considered as muti-micronuclei for the analysis).

Animal experiment—*Pten* was deleted in *Brca1* wildtype (M412) and *Brca1* heterozygous (M338) mOSE and mFTE lines. CRISPR/Cas9-GFP expressing plasmid were used to knockout *Pten* (Santa Cruz; Sc-422475) per manufacturer's protocol. FACS- based analysis was used to isolate Cas9-GFP (*Pten* knockout) expressing cell population and cells were seeded as single cells into a 96 well plate. Knockout was confirmed through western blot analysis.

The sgRNA sequence—sc-422475 A:

- Sense: ACCGCCAAATTTAACTGCAG

sc-422475 B:

- Sense: GCAGCAATTCACTGTAAAGC

sc-422475 C:

- Sense: AAAGCTGGAAAGGGACGGAC

For animal tumor study, mOSE and mFTE cells (TP-M412; *Brca1*$^{+/+}$ *Trp53*$^{-/-}$ *Pten*$^{-/-}$) and (BTP-M338; *Brca1*$^{+/-}$ *Trp53*$^{-/-}$ *Pten*$^{-/-}$) were injected either subcutaneously (n=4) or into the ovarian fat pad (OFP) of 6-weeks old NSG mice (n=6). For ovarian fat pad injections, mice were anesthetized with 1.25% Avertin, IP (4mg/10g body weight). Meloxicam and SR- buprenorphine analgesics were administered pre-operatively. While the mouse is anesthetized, its hair was shaved, and the incision site was cleaned with three rounds of a povidine iodine (Betadine scrub) and followed by a 70% alcohol rinse. A 1cm incision was made along the abdominal region between the third and fourth mammary gland roughly 0.5cm from the spine to expose the peritoneum where the ovary and ovarian fat pad are easily visible. A small incision was made in peritoneal wall above the ovary and ovarian fat depot. The adipose tissue and ovary were pulled through the peritoneal incision far enough to expose 0.5cm of adipose tissue. One million mOSE or mFTE lines in 1:1 ratio of PBS and Matrigel (Corning Matrigel; 354234) were injected in the ovarian fat pad with a Hamilton syringe. 25ul of cell/matrigel mixture was injected into ovarian fat pad of mice. After injection, the adipose depot was carefully pushed back through the peritoneal wall and sutured to close the peritoneum. The skin was gathered, and the incision was closed with wound clips. Following surgery, mice were kept warm on a heating pad until fully recovered. Meloxicam was used perioperatively, injected subcutaneously (5 mg/kg, s.c.), and was again followed up 24 hours later with a post-op administration, as per CAC guidelines for post-op care for animals undergoing survival surgery. For subcutaneous tumor model, we injected four million mOSE or mFTE cell lines into the right and left flanks of the NSG mice. Both OFP and subcutaneously injected mice were sacrificed when the biggest tumor reached 2cm which was in 1 month and 18 days after the injection. Tumors were collected and weights (g) were calculated.

QUANTIFICATION AND STATISTICAL ANALYSIS

Student t-test analysis was performed to calculate P-value for all the experiments using excel and/or GraphPad Prism. *, **, ***, and **** represents $P \leq 0.05$, $P \leq 0.01$, $P \leq 0.001$, and $P \leq 0.0001$ respectively. Additionally, independent t-test and verified by the non-parametric Mann-Whitney test was performed due small sample size. We also used mixed linear model to take the dependence within the person when comparing two groups to achieve statistical analysis of 53BP1 levels in the human OSE and FTE sections.

Supplementary Material

Refer to Web version on PubMed Central for supplementary material.

ACKNOWLEDGMENTS

We thank Dr. Jae-hoon Kim for providing human ovarian epithelial cells (IHOSE1431) and Dr. Ronny Drapkin for providing human fallopian tube epithelial cell lines (HFTE237 and HFTE194). We also thank Dr. Joanna Burdette for sharing the CD1 oviductal line for our analysis.[70] We thank Joshua Rivera for his technical support in helping us analyze immunohistochemistry data, Stevenson V. Tran with setting up mouse mating, and Dr. David Livingston's group for providing the mouse Brca1 antibody. We would like to express our sincere gratitude to the women who generously provided consent for the use of their prophylactic ovarian and fallopian tissue in our

research studies. Work on this project was supported by the Dana-Farber Cancer Institute Susan F. Smith Center for Women's Cancers (S.P.), 1P50CA240243 Ovarian SPORE from the NCI (C.C.), Foundation for Women's Wellness (S.P.), as well as a Proposal Development Grant (S.P.),and a CSM/ORSP micro-seed grant (S.P.) from the University of Massachusetts Boston.

REFERENCES

1. Kim J, Park EY, Kim O, Schilder JM, Coffey DM, Cho CH, and Bast RC Jr. (2018). Cell Origins of High-Grade Serous Ovarian Cancer. Cancers 10, 433. 10.3390/cancers10110433. [PubMed: 30424539]
2. Lheureux S, Braunstein M, and Oza AM (2019). Epithelial ovarian cancer: Evolution of management in the era of precision medicine. CA A Cancer J. Clin. 69, 280–304. 10.3322/caac.21559.
3. Peres LC, Cushing-Haugen KL, Köbel M, Harris HR, Berchuck A, Rossing MA, Schildkraut JM, and Doherty JA (2019). Invasive Epithelial Ovarian Cancer Survival by Histotype and Disease Stage. J. Natl. Cancer Inst. 111, 60–68. 10.1093/jnci/djy071. [PubMed: 29718305]
4. Bowtell DD, Böhm S, Ahmed AA, Aspuria PJ, Bast RC Jr., Beral V, Berek JS, Birrer MJ, Blagden S, Bookman MA, et al. (2015). Rethinking ovarian cancer II: reducing mortality from high-grade serous ovarian cancer. Nat. Rev. Cancer 15, 668–679. 10.1038/nrc4019. [PubMed: 26493647]
5. Morden CR, Farrell AC, Sliwowski M, Lichtensztejn Z, Altman AD, Nachtigal MW, and McManus KJ (2021). Chromosome instability is prevalent and dynamic in high-grade serous ovarian cancer patient samples. Gynecol. Oncol. 161, 769–778. 10.1016/j.ygyno.2021.02.038. [PubMed: 33714608]
6. Takaya H, Nakai H, Takamatsu S, Mandai M, and Matsumura N. (2020). Homologous recombination deficiency status-based classification of high-grade serous ovarian carcinoma. Sci. Rep. 10, 2757. 10.1038/s41598-020-59671-3. [PubMed: 32066851]
7. Cancer Genome Atlas Research Network (2011). Integrated genomic analyses of ovarian carcinoma. Nature 474, 609–615. 10.1038/nature10166. [PubMed: 21720365]
8. Iijima M, Banno K, Okawa R, Yanokura M, Iida M, Takeda T, Kunitomi-Irie H, Adachi M, Nakamura K, Umene K, et al. (2017). Genome-wide analysis of gynecologic cancer: The Cancer Genome Atlas in ovarian and endometrial cancer. Oncol. Lett. 13, 1063–1070. 10.3892/ol.2017.5582. [PubMed: 28454214]
9. Konstantinopoulos PA, Ceccaldi R, Shapiro GI, and D'Andrea AD (2015). Homologous Recombination Deficiency: Exploiting the Fundamental Vulnerability of Ovarian Cancer. Cancer Discov. 5, 1137–1154. 10.1158/2159-8290.CD-15-0714. [PubMed: 26463832]
10. Ledermann JA, Drew Y, and Kristeleit RS (2016). Homologous recombination deficiency and ovarian cancer. Eur. J. Cancer 60, 49–58. 10.1016/j.ejca.2016.03.005. [PubMed: 27065456]
11. Chiappa M, Guffanti F, Bertoni F, Colombo I, and Damia G. (2021). Overcoming PARPi resistance: Preclinical and clinical evidence in ovarian cancer. Drug Resist. Updates 55, 100744. 10.1016/j.drup.2021.100744.
12. Kolinjivadi AM, Sannino V, de Antoni A, Técher H, Baldi G, and Costanzo V. (2017). Moonlighting at replication forks - a new life for homologous recombination proteins BRCA1, BRCA2 and RAD51. FEBS Lett. 591, 1083–1100. 10.1002/1873-3468.12556. [PubMed: 28079255]
13. Saxena S, and Zou L. (2022). Hallmarks of DNA replication stress. Mol.Cell 82, 2298–2314. 10.1016/j.molcel.2022.05.004. [PubMed: 35714587]
14. He Y, Rivera J, Diossy M, Duan H, Bowman-Colin C, Reed R, Jennings R, Novak J, Tran SV, Cohen EF, et al. (2021). BRCA1/Trp53 heterozygosity and replication stress drive esophageal cancer development in a mouse model. Proc. Natl. Acad. Sci. USA 118, e2108421118. 10.1073/pnas.2108421118.
15. Auersperg N. (2013). Ovarian surface epithelium as a source of ovarian cancers: unwarranted speculation or evidence-based hypothesis? Gynecol. Oncol. 130, 246–251. 10.1016/j.ygyno.2013.03.021. [PubMed: 23558054]
16. Dinh HQ, Lin X, Abbasi F, Nameki R, Haro M, Olingy CE, Chang H, Hernandez L, Gayther SA, Wright KN, et al. (2021). Single-cell transcriptomics identifies gene expression networks

driving differentiation and tumorigenesis in the human fallopian tube. Cell Rep. 35, 108978. 10.1016/j.celrep.2021.108978.

17. Wang Y, Li L, Wang Y, Tang SN, and Zheng W. (2015). Fallopian tube secretory cell expansion-a sensitive biomarker for ovarian serous carcinogenesis.pdf. Am. J. Transl. Res. 7, 2082–2090. [PubMed: 26692952]
18. Lee Y, Miron A, Drapkin R, Nucci MR, Medeiros F, Saleemuddin A, Garber J, Birch C, Mou H, Gordon RW, et al. (2007). A candidate precursor to serous carcinoma that originates in the distal fallopian tube. J. Pathol. 211, 26–35. 10.1002/path.2091. [PubMed: 17117391]
19. Karst AM, and Drapkin R. (2010). Ovarian cancer pathogenesis: a model in evolution. JAMA Oncol. 2010, 932371. 10.1155/2010/932371.
20. Callahan MJ, Crum CP, Medeiros F, Kindelberger DW, Elvin JA, Garber JE, Feltmate CM, Berkowitz RS, and Muto MG (2007). Primary fallopian tube malignancies in BRCA-positive women undergoing surgery for ovarian cancer risk reduction. J. Clin. Oncol. 25, 3985–3990. 10.1200/JCO.2007.12.2622. [PubMed: 17761984]
21. Bachert SE, McDowell A Jr., Piecoro D, and Baldwin Branch L. (2020). Serous Tubal Intraepithelial Carcinoma: A Concise Review for the Practicing Pathologist and Clinician. Diagnostics 10, 102. 10.3390/diagnostics10020102. [PubMed: 32069831]
22. Kuhn E, Kurman RJ, Vang R, Sehdev AS, Han G, Soslow R, Wang TL, and Shih IM (2012). TP53 mutations in serous tubal intraepithelial carcinoma and concurrent pelvic high-grade serous carcinoma–evidence supporting the clonal relationship of the two lesions. J. Pathol. 226, 421–426. 10.1002/path.3023. [PubMed: 21990067]
23. Ducie J, Dao F, Considine M, Olvera N, Shaw PA, Kurman RJ, Shih IM, Soslow RA, Cope L, and Levine DA (2017). Molecular analysis of high-grade serous ovarian carcinoma with and without associated serous tubal intra-epithelial carcinoma. Nat. Commun. 8, 990. 10.1038/s41467-017-01217-9. [PubMed: 29042553]
24. Eckert MA, Pan S, Hernandez KM, Loth RM, Andrade J, Volchenboum SL, Faber P, Montag A, Lastra R, Peter ME, et al. (2016). Genomics of Ovarian Cancer Progression Reveals Diverse Metastatic Trajectories Including Intraepithelial Metastasis to the Fallopian Tube. Cancer Discov. 6, 1342–1351. 10.1158/2159-8290.CD-16-0607. [PubMed: 27856443]
25. Labidi-Galy SI, Papp E, Hallberg D, Niknafs N, Adleff V, Noe M, Bhattacharya R, Novak M, Jones S, Phallen J, et al. (2017). High grade serous ovarian carcinomas originate in the fallopian tube. Nat. Commun. 8, 1093. 10.1038/s41467-017-00962-1. [PubMed: 29061967]
26. Lõhmussaar K, Kopper O, Korving J, Begthel H, Vreuls CPH, van Es JH, and Clevers H. (2020). Assessing the origin of high-grade serous ovarian cancer using CRISPR-modification of mouse organoids. Nat. Commun. 11, 2660. 10.1038/s41467-020-16432-0. [PubMed: 32461556]
27. Zhang S, Dolgalev I, Zhang T, Ran H, Levine DA, and Neel BG (2019). Both fallopian tube and ovarian surface epithelium are cells-of-origin for high-grade serous ovarian carcinoma. Nat. Commun. 10, 5367. 10.1038/s41467-019-13116-2. [PubMed: 31772167]
28. Bowman-Colin C, Xia B, Bunting S, Klijn C, Drost R, Bouwman P, Fineman L, Chen X, Culhane AC, Cai H, et al. (2013). Palb2 synergizes with Trp53 to suppress mammary tumor formation in a model of inherited breast cancer. Proc. Natl. Acad. Sci. USA 110, 8632–8637. 10.1073/pnas.1305362110. [PubMed: 23657012]
29. Tallquist MD, and Soriano P. (2000). Epiblast-Restricted Cre Expression in MORE Mice- A Tool to Distinguish Embryonic vs. Extra-Embryonic Gene Function. Genesis 26, 113–115. [PubMed: 10686601]
30. Perets R, Wyant GA, Muto KW, Bijron JG, Poole BB, Chin KT, Chen JYH, Ohman AW, Stepule CD, Kwak S, et al. (2013). Transformation of the fallopian tube secretory epithelium leads to high-grade serous ovarian cancer in Brca;Tp53;Pten models. Cancer Cell 24, 751–765. 10.1016/j.ccr.2013.10.013. [PubMed: 24332043]
31. Chaves-Moreira D, et al. (2020). PAX8 ochestrates an angiogenic program through interaction with Sox17. Preprint at bioRxiv. 10.1101/2020.09.09.290387.
32. Pathania S, Bade S, Le Guillou M, Burke K, Reed R, Bowman-Colin C, Su Y, Ting DT, Polyak K, Richardson AL, et al. (2014). BRCA1 haploinsufficiency for replication stress suppression in primary cells. Nat. Commun. 5, 5496. 10.1038/ncomms6496. [PubMed: 25400221]

33. Zou L, and Elledge SJ (2003). J. Sensing DNA Damage Through ATRIP Recognition of RPA-ssDNA Complexes.pdf. Science 300, 1542–1548. [PubMed: 12791985]
34. Maréchal A, and Zou L. (2015). RPA-coated single-stranded DNA as a platform for post-translational modifications in the DNA damage response. Cell Res. 25, 9–23. 10.1038/cr.2014.147. [PubMed: 25403473]
35. Blackford AN, Jackson SP, ATM ATR, and DNA- PK (2017). The Trinity at the Heart of the DNA Damage Response. Mol. Cell 66, 801–817. 10.1016/j.molcel.2017.05.015. [PubMed: 28622525]
36. Pathania S, Nguyen J, Hill SJ, Scully R, Adelmant GO, Marto JA, Feunteun J, and Livingston DM (2011). BRCA1 is required for postreplication repair after UV-induced DNA damage. Mol. Cell 44, 235–251. 10.1016/j.molcel.2011.09.002. [PubMed: 21963239]
37. Xu Y, Ning S, Wei Z, Xu R, Xu X, Xing M, Guo R, and Xu D. (2017). 53BP1 and BRCA1 control pathway choice for stalled replication restart. Elife 6, e30523. 10.7554/eLife.30523.
38. Qinghua L, et al. (2000). Chk1 is an essential kinase that is regulated by Atr and required for the G2:M DNA damage checkpoint. Gene Dev., 1448–1459. [PubMed: 10859164]
39. Bartek J, and Lukas J. (2003). Chk1 and Chk2 kinases in checkpoint control and cancer.pdf. Cancer Cell 3, 421–429. [PubMed: 12781359]
40. Crosio C, Fimia GM, Loury R, Kimura M, Okano Y, Zhou H, Sen S, Allis CD, and Sassone-Corsi P. (2002). Mitotic phosphorylation of histone H3: spatio-temporal regulation by mammalian Aurora kinases. Mol. Cell Biol. 22, 874–885. 10.1128/MCB.22.3.874-885.2002. [PubMed: 11784863]
41. Hatch EM, and Hetzer MW (2015). Linking Micronuclei to Chromosome Fragmentation. Cell 161, 1502–1504. 10.1016/j.cell.2015.06.005. [PubMed: 26091034]
42. Martins FC, Couturier DL, Paterson A, Karnezis AN, Chow C, Nazeran TM, Odunsi A, Gentry-Maharaj A, Vrvilo A, Hein A, et al. (2020). Clinical and pathological associations of PTEN expression in ovarian cancer: a multicentre study from the Ovarian Tumour Tissue Analysis Consortium. Br. J. Cancer 123, 793–802. 10.1038/s41416-020-0900-0. [PubMed: 32555365]
43. Wu R, Baker SJ, Hu TC, Norman KM, Fearon ER, and Cho KR (2013). Type I to type II ovarian carcinoma progression: mutant Trp53 or Pik3ca confers a more aggressive tumor phenotype in a mouse model of ovarian cancer. Am. J. Pathol. 182, 1391–1399. 10.1016/j.ajpath.2012.12.031. [PubMed: 23499052]
44. Nomani A, Li G, Yousefi S, Wu S, Malekshah OM, Nikkhoi SK, Pourfathi M, Rizi R, and Hatefi A. (2021). Gadolinium-labeled affibody-XTEN recombinant vector for detection of HER2+ lesions of ovarian cancer lung metastasis using quantitative MRI. J. Contr. Release 337, 132–143. 10.1016/j.jconrel.2021.07.022.
45. Zhang D, Wang Y, Dong L, Huang Y, Yuan J, Ben W, Yang Y, Ning N, Lu M, and Guan Y. (2013). Therapeutic role of EF24 targeting glucose transporter 1-mediated metabolism and metastasis in ovarian cancer cells. Cancer Sci. 104, 1690–1696. 10.1111/cas.12293. [PubMed: 24112101]
46. Li NF, Broad S, Lu YJ, Yang JS, Watson R, Hagemann T, Wilbanks G, Jacobs I, Balkwill F, Dafou D, and Gayther SA (2007). Human ovarian surface epithelial cells immortalized with hTERT maintain functional pRb and p53 expression.pdf. Cell Prolif. 40, 780–794. [PubMed: 17877616]
47. Shin HY, Yang W, Lee EJ, Han GH, Cho H, Chay DB, and Kim JH (2018). Establishment of five immortalized human ovarian surface epithelial cell lines via SV40 T antigen or HPV E6/E7 expression. PLoS One 13, e0205297. 10.1371/journal.pone.0205297.
48. Karst AM, and Drapkin R. (2012). Primary culture and immortalization ofhuman fallopian tube secretory epithelial cells. Nat. Protoc. 7, 1755–1764. 10.1038/nprot.2012.097. [PubMed: 22936217]
49. Karst AM, Levanon K, and Drapkin R. (2011). Modeling high-grade serous ovarian carcinogenesis from the fallopian tube. Proc. Natl. Acad. Sci. USA 108, 7547–7552. 10.1073/pnas.1017300108. [PubMed: 21502498]
50. Her J, Ray C, Altshuler J, Zheng H, and Bunting SF (2018). 53BP1 Mediates ATR-Chk1 Signaling and Protects Replication Forks under Conditions of Replication Stress.pdf. Mol. Cell Biol. 38, 004722-e517. 10.101128/MCB.
51. King SM, Hilliard TS, Wu LY, Jaffe RC, Fazleabas AT, and Burdette JE (2011). The impact of ovulation on fallopian tube epithelial cells: evaluating three hypotheses connecting ovulation

and serous ovarian cancer. Endocr. Relat. Cancer 18, 627–642. 10.1530/erc-11-0107. [PubMed: 21813729]

52. Eddie SL, Quartuccio SM, Zhu J, Shepherd JA, Kothari R, Kim JJ, Woodruff TK, and Burdette JE (2015). Three-dimensional modeling of the human fallopian tube fimbriae. Gynecol. Oncol. 136, 348–354. 10.1016/j.ygyno.2014.12.015. [PubMed: 25527363]
53. McLemore MR, Miaskowski C, Aouizerat BE, Chen LM, and Dodd MJ (2009). Epidemiological and genetic factors associated with ovarian cancer. Cancer Nurs. 32, 281–288, ; quiz 289–90; quiz 289–290. 10.1097/NCC.0b013e31819d30d6. [PubMed: 19444085]
54. Treviño LS, Buckles EL, and Johnson PA (2012). Oral contraceptives decrease the prevalence of ovarian cancer in the hen. Cancer Prev. Res. 5, 343–349. 10.1158/1940-6207.CAPR-11-0344.
55. Sasamoto N, Stewart PA, Wang T, Yoder SJ, Chellappan S, Hecht JL, Fridley BL, Terry KL, and Tworoger SS (2022). Lifetime ovulatory years and ovarian cancer gene expression profiles. J. Ovarian Res. 15, 59. 10.1186/s13048-022-00995-1(2022. [PubMed: 35562768]
56. Flesken-Nikitin A, Hwang CI, Cheng CY, Michurina TV, Enikolopov G, and Nikitin AY (2013). Ovarian surface epithelium at the junction area contains a cancer-prone stem cell niche. Nature 495, 241–245. 10.1038/nature11979. [PubMed: 23467088]
57. Coscia F, Watters KM, Curtis M, Eckert MA, Chiang CY, Tyanova S, Montag A, Lastra RR, Lengyel E, and Mann M. (2016). Integrative proteomic profiling of ovarian cancer cell lines reveals precursor cell associated proteins and functional status. Nat. Commun. 7, 12645. 10.1038/ncomms12645. [PubMed: 27561551]
58. Hao D, Li J, Jia S, Meng Y, Zhang C, Wang L, and Di LJ (2017). Integrated Analysis Reveals Tubal- and Ovarian-Originated Serous Ovarian Cancer and Predicts Differential Therapeutic Responses. Clin. Cancer Res. 23, 7400–7411. 10.1158/1078-0432.CCR-17-0638. [PubMed: 28939742]
59. Chien J, Sicotte H, Fan JB, Humphray S, Cunningham JM, Kalli KR, Oberg AL, Hart SN, Li Y, Davila JI, et al. (2015). TP53 mutations, tetraploidy and homologous recombination repair defects in early stage high-grade serous ovarian cancer. Nucleic Acids Res. 43, 6945–6958. 10.1093/nar/gkv111. [PubMed: 25916844]
60. Milanesio MC, Giordano S, and Valabrega G. (2020). Clinical Implications of DNA Repair Defects in High-Grade Serous Ovarian Carcinomas. Cancers 12, 1315. 10.3390/cancers12051315. [PubMed: 32455819]
61. Gaillard H, García-Muse T, and Aguilera A. (2015). Replication stress and cancer. Nat. Rev. Cancer 15, 276–289. 10.1038/nrc3916. [PubMed: 25907220]
62. Macheret M, and Halazonetis TD (2015). DNA replication stress as a hallmark of cancer. Annu. Rev. Pathol. 10, 425–448. 10.1146/annurev-pathol-012414-040424. [PubMed: 25621662]
63. Gralewska P, Gajek A, Marczak A, and Rogalska A. (2020). Participation of the ATR/CHK1 pathway in replicative stress targeted therapy of high-grade ovarian cancer. J. Hematol. Oncol. 13, 39. 10.1186/s13045-020-00874-6. [PubMed: 32316968]
64. Konstantinopoulos PA, da Costa AABA, Gulhan D, Lee EK, Cheng SC, Hendrickson AEW, Kochupurakkal B, Kolin DL, Kohn EC, Liu JF, et al. (2021). A Replication stress biomarker is associated with response to gemcitabine versus combined gemcitabine and ATR inhibitor therapy in ovarian cancer. Nat. Commun. 12, 5574. 10.1038/s41467-021-25904-w(2021. [PubMed: 34552099]
65. Ngoi NY, Sundararajan V, and Tan DS (2020). Exploiting replicative stress in gynecological cancers as a therapeutic strategy. Int. J. Gynecol. Cancer 30, 1224–1238. 10.1136/ijgc-2020-001277. [PubMed: 32571890]
66. Pakneshan S, Safarpour D, Tavassoli F, and Jabbari B. (2014). Brain metastasis from ovarian cancer: a systematic review. J. Neuro Oncol. 119, 1–6. 10.1007/s11060-014-1447-9.
67. Borella F, Bertero L, Morrone A, Gambella A, Bovetti M, Cosma S, Carosso A, Katsaros D, Gemmiti S, Preti M, et al. (2020). Brain Metastases from Ovarian Cancer: Current Evidence in Diagnosis, Treatment, and Prognosis. Cancers 12, 2156. 10.3390/cancers12082156. [PubMed: 32759682]

68. Palma-Vera SE, Schoen J, and Chen S. (2017). Periovulatory follicular fluid levels of estradiol trigger inflammatory and DNA damage responses in oviduct epithelial cells. PLoS One 12, e0172192. 10.1371/journal.pone.0172192.

69. Pennington KP, Wickramanayake A, Norquist BM, Pennil CC, Garcia RL, Agnew KJ, Taniguchi T, Welcsh P, and Swisher EM (2013). 53BP1 expression in sporadic and inherited ovarian carcinoma: Relationship to genetic status and clinical outcomes. Gynecol. Oncol. 128, 493–499. 10.1016/j.ygyno.2012.12.007. [PubMed: 23246380]

70. Endsley MP, Moyle-Heyrman G, Karthikeyan S, Lantvit DD, Davis DA, Wei JJ, and Burdette JE (2015). Spontaneous Transformation of Murine Oviductal Epithelial Cells: A Model System to Investigate the Onset of Fallopian-Derived Tumors. Front. Oncol. 5, 154. 10.3389/fonc.2015.00154.

71. Liu X, Holstege H, van der Gulden H, Treur-Mulder M, Zevenhoven J, Velds A, Kerkhoven RM, van Vliet MH, Wessels LFA, Peterse JL, et al. (2007). Somatic loss of BRCA1 and p53 in mice induces mammary tumors with features of human BRCA1-mutated basal-like breast cancer. Proc. Natl. Acad. Sci. USA 104, 12111–12116. 10.1073/pnas.0702969104. [PubMed: 17626182]

72. King SM, Quartuccio SM, Vanderhyden BC, and Burdette JE(2013). Early transformative changes in normal ovarian surface epithelium induced by oxidative stress require Akt upregulation, DNA damage and epithelial-stromal interaction. Carcinogenesis 34, 1125–1133. 10.1093/carcin/bgt003. [PubMed: 23299406]

73. Roby KF, Taylor CC, Sweetwood JP, Cheng Y, Pace JL, Tawfik O, Persons DL, Smith PG, and Terranova PF (2000). Development of a syngeneic mouse model for events related to ovarian cancer. Carcinogenesis 21, 585–591. [PubMed: 10753190]

74. Umezu T, Hanazono M, Aizawa S, and Tomooka Y. (2003). Characterization of newly established clonal oviductal cell lines and differential hormonal regulation of gene expression. In Vitro Cell. Dev. Biol. Anim. 39, 146–156. 10.1290/0305036.i. [PubMed: 14505432]

75. Clark-Knowles KV, Garson K, Jonkers J, and Vanderhyden BC (2007). Conditional inactivation of Brca1 in the mouse ovarian surface epithelium results in an increase in preneoplastic changes. Exp. Cell Res. 313, 133–145. 10.1016/j.yexcr.2006.09.026. [PubMed: 17070800]

76. Kindelberger DW, Lee Y, Miron A, Hirsch MS, Feltmate C, Medeiros F, Callahan MJ, Garner EO, Gordon RW, Birch C, et al. (2007). Intraepithelial Carcinoma of the Fimbria and Pelvic Serous Carcinoma- Evidence for a Causal Relationship.pdf. Am. J. Surg. Pathol. 31, 161–169. [PubMed: 17255760]

Highlights

- FTE cells show higher replication stress, genomic instability, and tumorigenicity than OSEs
- Brca1 heterozygous OSE/FTE cells are haploinsufficient for replication stress suppression
- Human/mouse FT epithelium has higher 53BP1 signal/replication stress than OS epithelium
- Fimbrial ends are replication stress prone and the stress extent is influenced by menopause

A

Cell lines	p53 status	Genotype
M412 (mOSE)	$p53^{-/-}$	$Trp53^{flox/del}$;$Meox2^{wt/Cre}$
M412 (mFTE)	$p53^{-/-}$	$Trp53^{flox/del}$;$Meox2^{wt/Cre}$
M56 (mOSE)	$p53^{-/-}$	$Trp53^{del/del}$;$Meox2^{wt/wt}$
M56 (mFTE)	$p53^{-/-}$	$Trp53^{del/del}$;$Meox2^{wt/wt}$

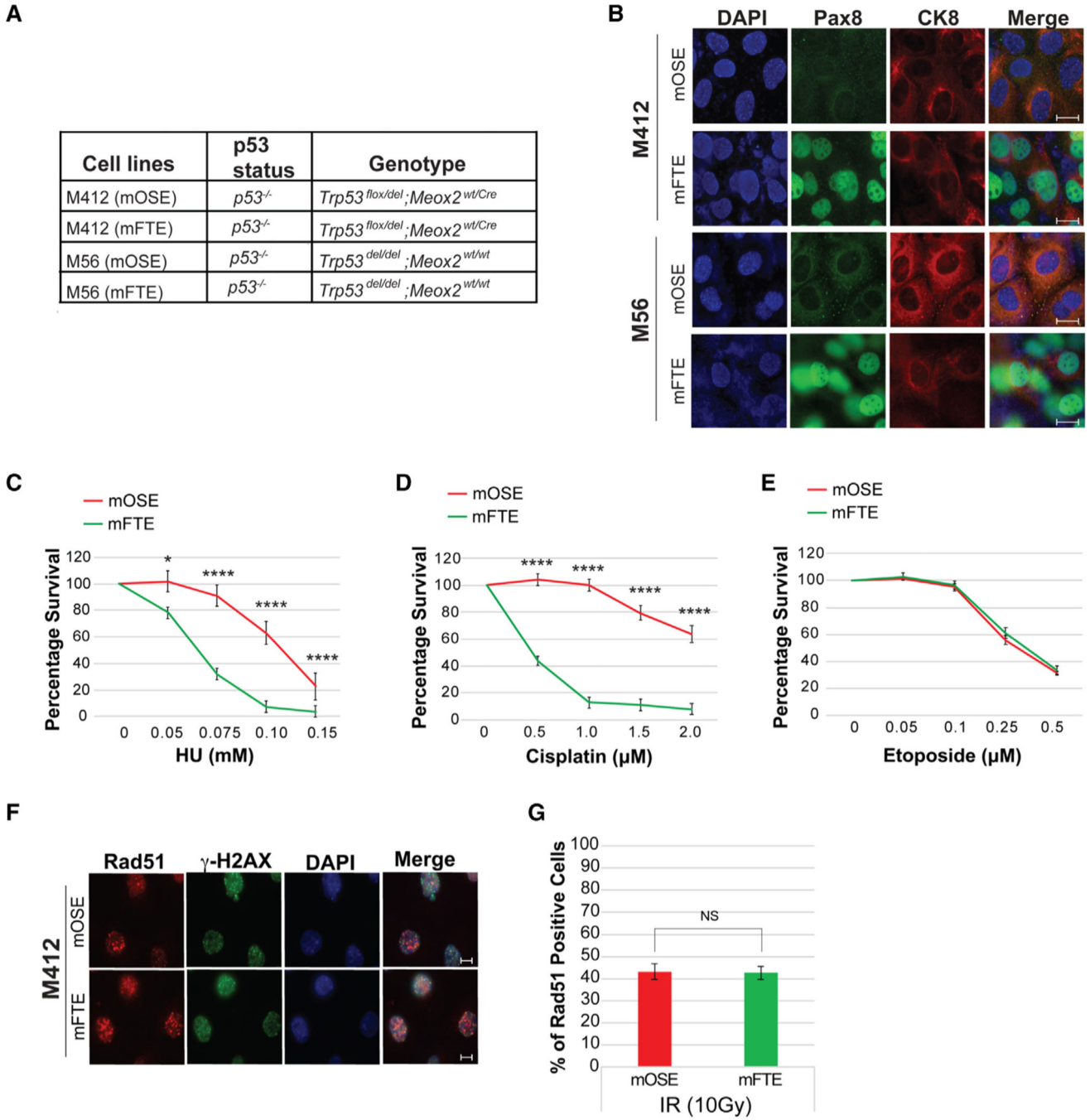

Figure 1. Characterization of isogenic pairs of mOSE and mFTE cell lines and their sensitivity to different DNA-damaging agents

(A) Summary of genotypes of isogenic pairs of mOSE and mFTE lines generated from two genetically modified mice (M412 and M56).

(B) Representative immunofluorescence images for CK8 and Pax8 in mOSE and mFTE cells from M412 and M56 mice. Images were taken at 63× magnification, and the scale bar represents 20 μm.

(C–E) CellTiter-Glo-based cell survival assays. (C) Cells were treated with HU for 3 days and collected 2 days post-HU treatment. (D) Cisplatin was added for 24 h and cells were

collected for analysis 4 days post-treatment. (E) Cells were treated with etoposide for 3 days at indicated doses and collected for analysis 2 days later. Error bars represent SD between triplicates. *$p \leq 0.05$ and ****$p \leq 0.0001$.

(F and G) mOSE and mFTE cells (M412) were irradiated (10 Gy) and analyzed 4 h later for Rad51 and γ-H2AX focus-positive cells. Representative immuno-fluorescence images are shown in (F) and quantification is shown in (G). Two hundred cells/experiment were counted for this analysis. Error bars indicate the SD between three biological replicates. NS indicates not significant. Images were taken at 63×, and the scale represents 20 μm.

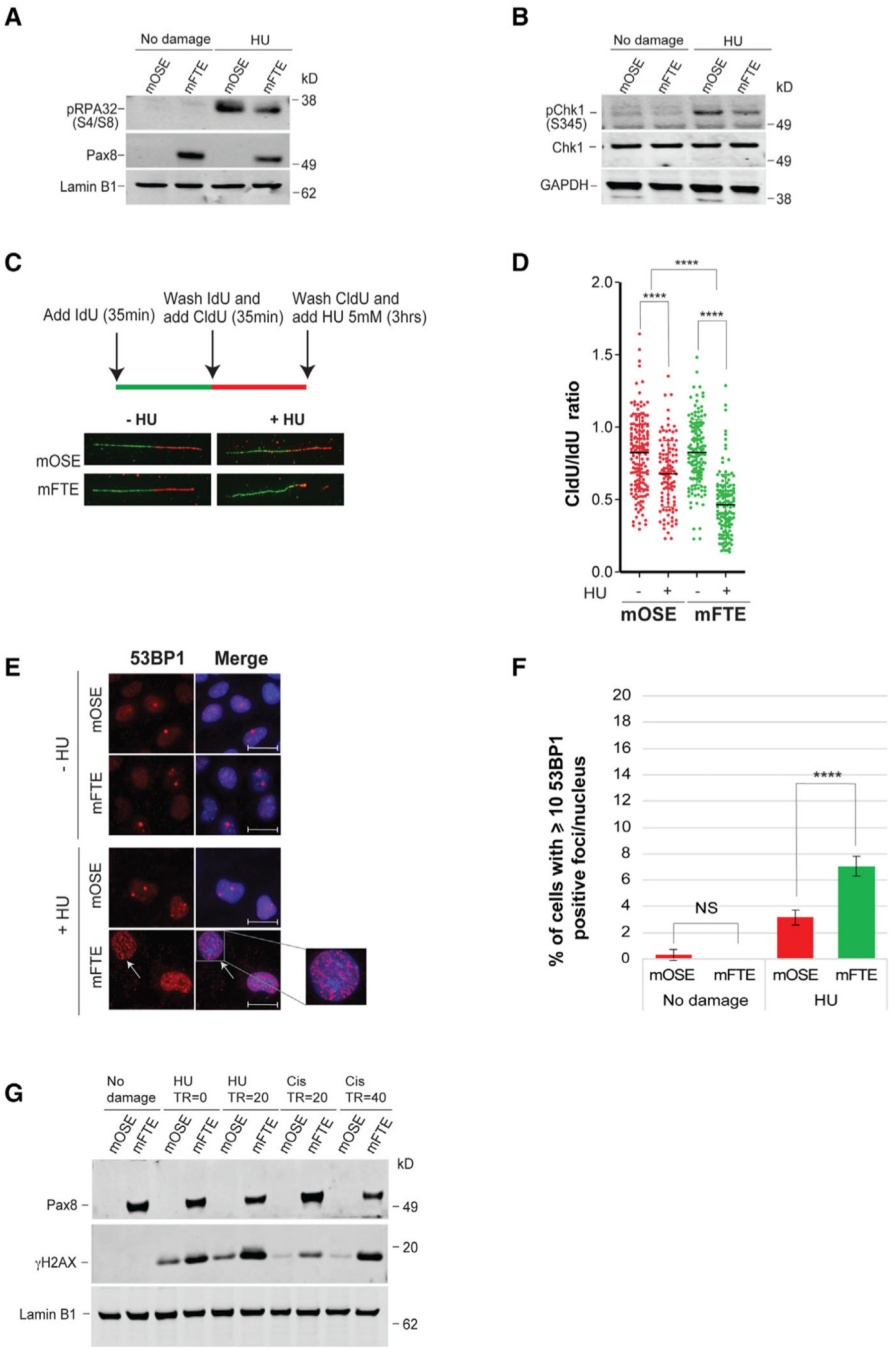

Figure 2. mFTE cells show defective stalled fork repair and increased DNA damage accumulation upon replication stress

(A) Nuclear extracts were analyzed for accumulation of pRPA (S4/S8). Cells were treated with 5 mM HU for 3 h.

(B) Western blot analysis of cytoplasmic pChk1 (S345) and Chk1 levels in cells treated with 5 mM HU for 3 h.

(C) Schematic overview of DNA fiber assay (top) and representative tracts (bottom) from cells grown in the presence or absence of 5 mM HU for 3 h. Green and red tracts correspond to IdU and CldU incorporation, respectively.

(D) Scatterplots compare the ratios of CldU/IdU tract lengths in the presence and absence of HU. Black lines indicate the average. n ≥ 100 tracts were scored for each dataset. ****p ≤ 0.0001.

(E) Representative immunofluorescence (IF) images of cells scored for 53BP1 foci are shown. White arrow points to the 53BP1 foci positive nucleus which is magnified further in the side panel. Images were taken at 63× magnification. Scale bar represents 20 μm.

(F) The graph indicates the percentage of cells with 10 or more 53BP1 foci per nucleus. Error bars indicate the SD between two technical replicates of two biological experiments. NS indicates not significant, ****p ≤ 0.0001.

(G) Western blot analysis of γH2AX levels. Cells were treated with 5 mM HU for 3 h (TR = 0) and allowed to recover for 20 h (TR = 20) or treated with 25 μM cisplatin for 1 h and allowed to recover for 20 h (TR = 20) or 40 h (TR = 40).

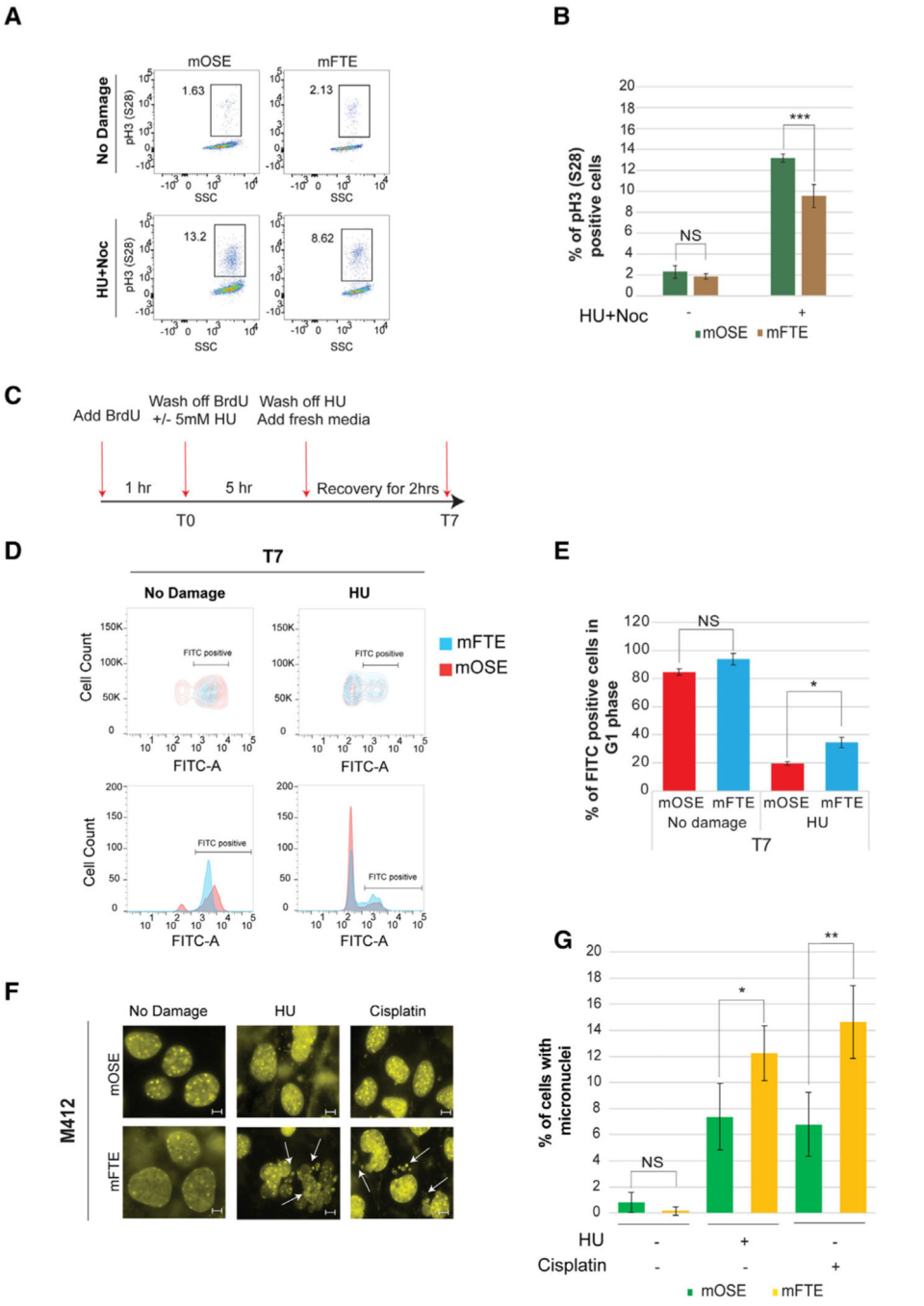

Figure 3. Defective G2/M checkpoint activation and micronucleus formation in mFTE cells compared with isogenic mOSE counterparts (M412)

(A and B) (A) FACS-based analysis of the mitotic populations in mOSE and mFTE lines treated with HU and nocodazole. Cells were cultured in the presence or absence of 2 mM HU for 5 h. After 5 h, HU was washed off, and the cells were incubated with 0.1 μg/mL nocodazole for 18 h. Cells were then fixed and stained with phospho-histone H3 (S28) antibody (mitosis-specific marker). (B) Percentage of pH3 (S28)-positive cells in mOSE and mFTE lines in the presence or absence of HU and nocodazole is plotted. Error bars indicate the SD between two biological replicates. NS indicates not significant and ***$p \leq 0.001$

(C) Experimental schematic of FACS-based G2/M checkpoint analysis of mOSE and mFTE cells in the presence or absence of HU.
(D and E) Cells were cultured in the presence of BrdU for 1 h (T0), followed by treatment with 5 mM HU for 5 h, and then allowed to recover for 2 h (T7) in fresh medium. The cells were harvested, fixed, and stained with BrdU antibody and propidium iodide.
(D) BrdU-positive cells (FITC-A) are plotted against forward scatter (FSC-A) in the top row and cell count is shown in the bottom row. (E) Data presented in (D) are plotted. Graph indicates the percentage of BrdU-positive cells (FITC-A) in G1 phase of the cell cycle in the presence or absence of HU (T7). Error bars indicate the SD between two biological replicates. NS indicates not significant and *$p \leq 0.05$.
(F) Increased micronucleus formation in mFTE cells compared with isogenic mOSE cells. Cells were treated with 2 μM cisplatin for 5 h and allowed to recover for 24 h or treated with 5 mM HU for 5 h and allowed to recover for 48 h before being fixed for micronucleus analysis. White arrows point out the cells with micronuclei. IF images were taken at 63× and scale bars represent 20 μm.
(G) Graph shows the percentage of cells with micro-nuclei post-cisplatin or HU treatment. Error bars indicate the SD between two technical replicates of two biological experiments. NS indicates not significant, *$p \leq 0.05$, **$p \leq 0.01$.

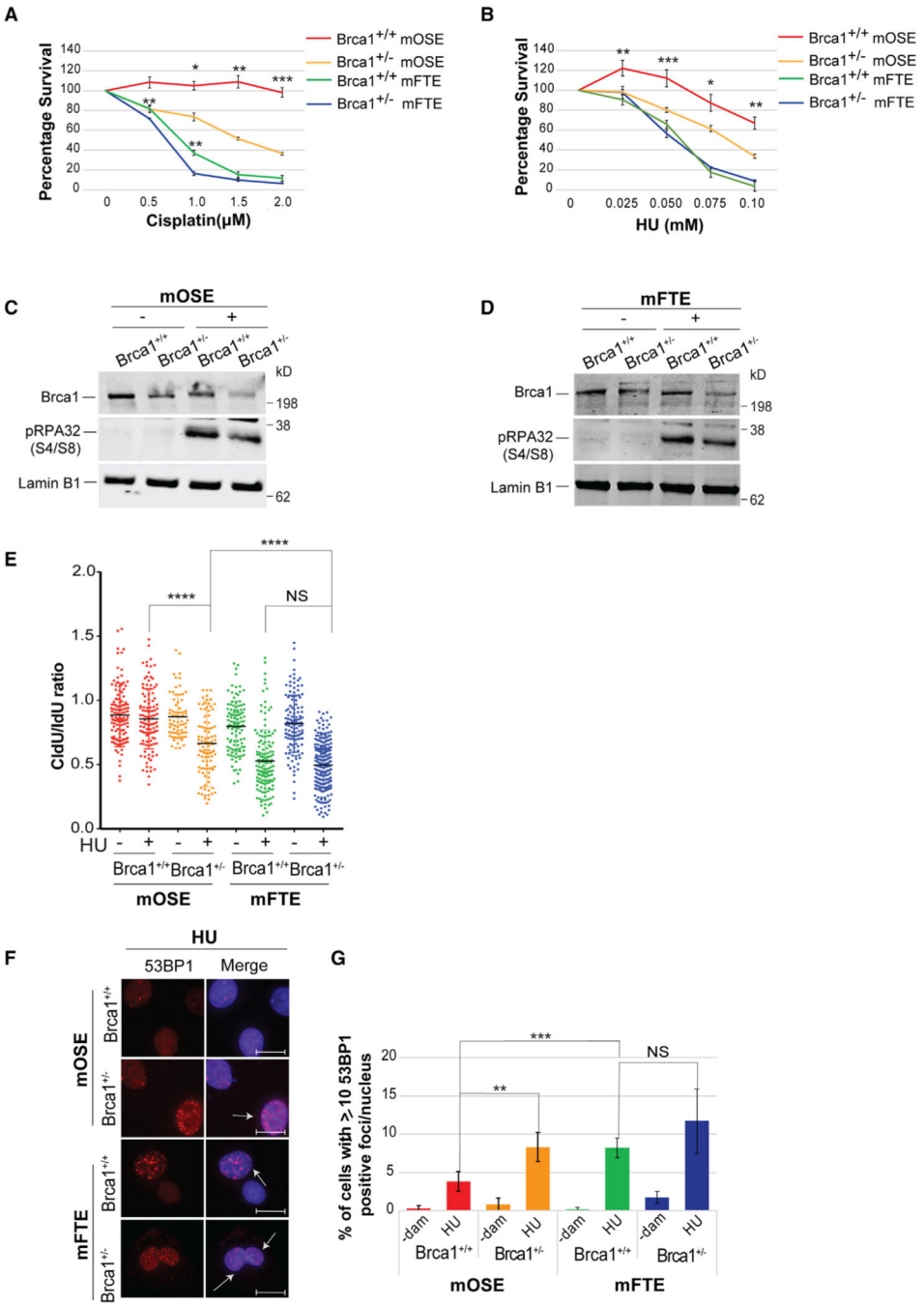

Figure 4. *Brca1* heterozygous mOSEs and mFTEs (M338) are haploinsufficient for stalled fork repair

(A and B) *Brca1* WT and heterozygous mOSE and mFTE cells were treated (A) with indicated doses of cisplatin for a day and (B) with HU for 3 days, and both treatments were allowed to recover for 4 days (cisplatin) and 2 days (HU). Cell viability was measured with the CellTiter-Glo-based cell survival assay. *p ≤ 0.05, **p ≤ 0.01, and ***p ≤ 0.001.

(C and D) Western blot analysis of nuclear extracts prepared from *Brca1* WT and heterozygous (C) mOSE and (D) mFTE cells undergoing HU-induced replication stress. Cells were treated with 5 mM HU for 3 h and collected thereafter to prepare nuclear

extracts. Western blots were probed with pRPA (S4/S8), Brca1, and Lamin B1 (loading control).

(E) Fiber-based assay to analyze fork degradation in *Brca1* WT (M412) and *Brca1* heterozygous (M338) mOSE and mFTE cells after HU treatment. Cells were sequentially labeled with IdU followed by CldU and then treated with 5 mM HU for 3 h. Ratio of CldU/IdU tract length is plotted. NS indicates not significant and ****$p \leq 0.0001$.

(F and G) *Brca1* heterozygous mOSE and mFTE cells are more prone to fork collapse than the *Brca1* WT cells. (F) Representative IF images and (G) graph of the percentage of 53BP1-positive *Brca1* heterozygous mOSE and mFTE cells. Cells were treated with 6 mM HU for 4 h and then allowed to recover for 18 h. Images were taken at 63× magnification. Scale bar in white represent 20 μm. Graph shows the percentage of cells with 10 or more 53BP1 foci per nucleus. Error bars indicate the SD between two technical replicates of two biological experiments. White arrows point to 53BP1 positive nuclei. IF images were taken at 63X and scale bars represent 20 μm. NS indicates not significant, **$p \leq 0.01$, ***$p \leq 0.001$.

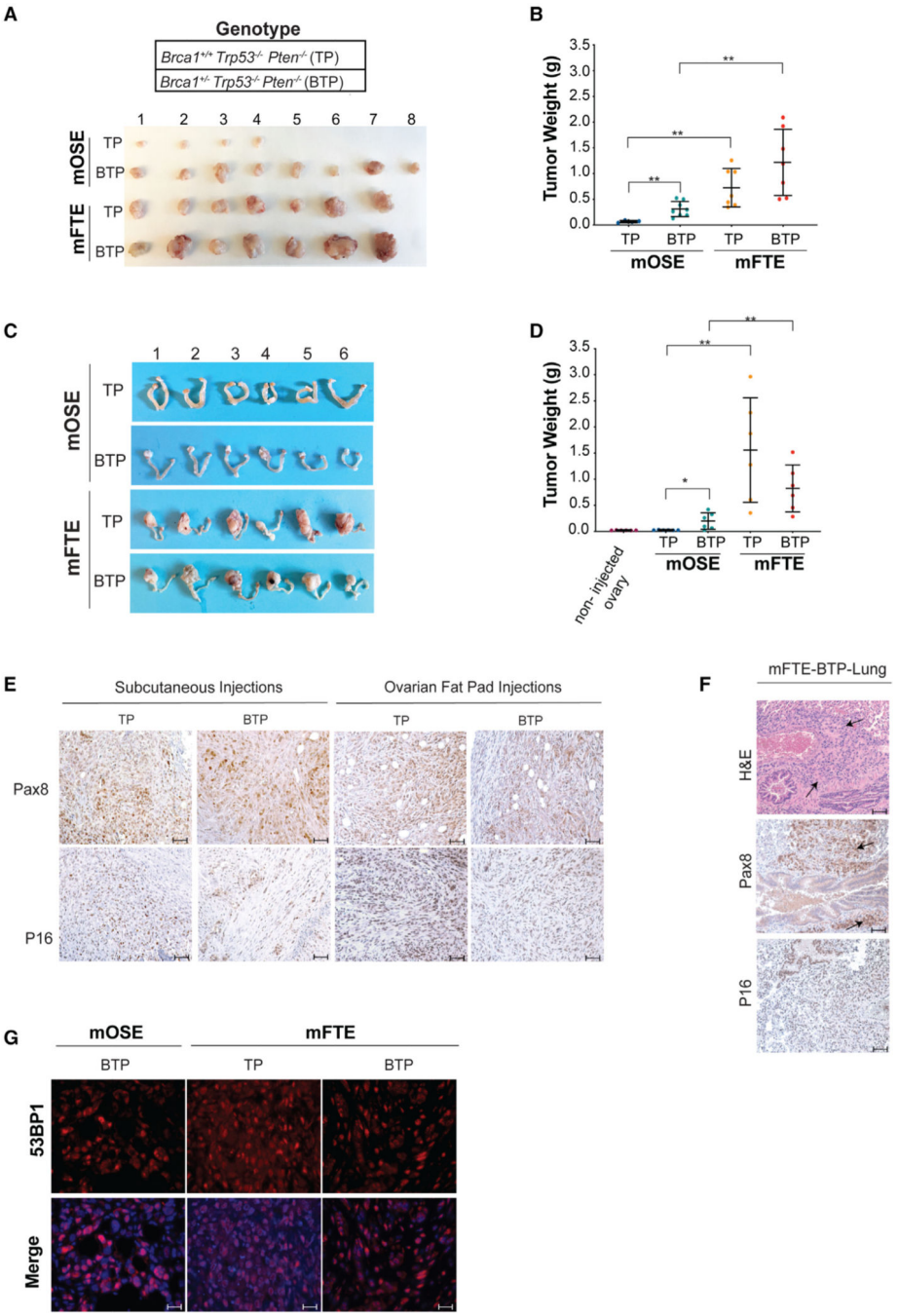

Figure 5. Fallopian tube epithelial cells are more prone to tumorigenesis than ovarian surface epithelial cells

(A and B) Four million cells each from four cell lines (2× mOSE and 2× mFTE) with the genotypes TP (*Brca1*$^{+/+}$; *Trp53*$^{-/-}$; *Pten*$^{-/-}$) and BTP (*Brca1*$^{+/-}$; *Trp53*$^{-/-}$; *Pten*$^{-/-}$) were subcutaneously injected into both flanks of 6-week-old NSG (NOD scid gamma; Prkdc^{scid} Il2rg^{tm1Wji}) mice. n = 4 mice (eight injection sites) per group were injected with the cells. (A) Tumors were harvested from all mice 48 days post-subcutaneous injections and (B) tumor weight was measured.

(C and D) One million TP and BTP cells (mOSE and mFTE lines) were injected into the ovarian fat pad of 6-week-old NSG mice (n = 6 mice per group). (C) Tumors were harvested 48 days post-ovarian fat pad injections and (D) weight of the tumors was measured. *$p \leq 0.05$ and **$p \leq 0.01$.

(E) Representative immunohistochemistry (IHC) sections assessing Pax8 and P16 expression in mFTE tumors harvested from both subcutaneous and ovarian fat pad injections. Images were taken at 20× magnification. Scale bar in black represents 50 μm.

(F) Lung metastasis of ovarian fat pad-injected *Brca1* heterozygous (BTP) mFTE lines. Representative lung H&E and IHC images of fallopian tube BTP mice. Black arrows point to tumor metastasis in lung tissue. Metastasized tumors stained positive for HGSOC markers Pax8 and P16. H&E and IHC images were taken at 20× magnification and scale bar represents 50 μm.

(G) Representative images of 53BP1-positive cells in mOSE (BTP) and mFTE (TP and BTP) tumor sections from ovarian fat pad-injected mice. IF images were taken at 63× magnification and scale bar represents 20 μm.

A

Cell lines	Modifications
IHOSE1431	SV40 TAg
HOSE	hTERT
HFTE237	SV40 TAg, hTERT
HFTE194	SV40 TAg, hTERT

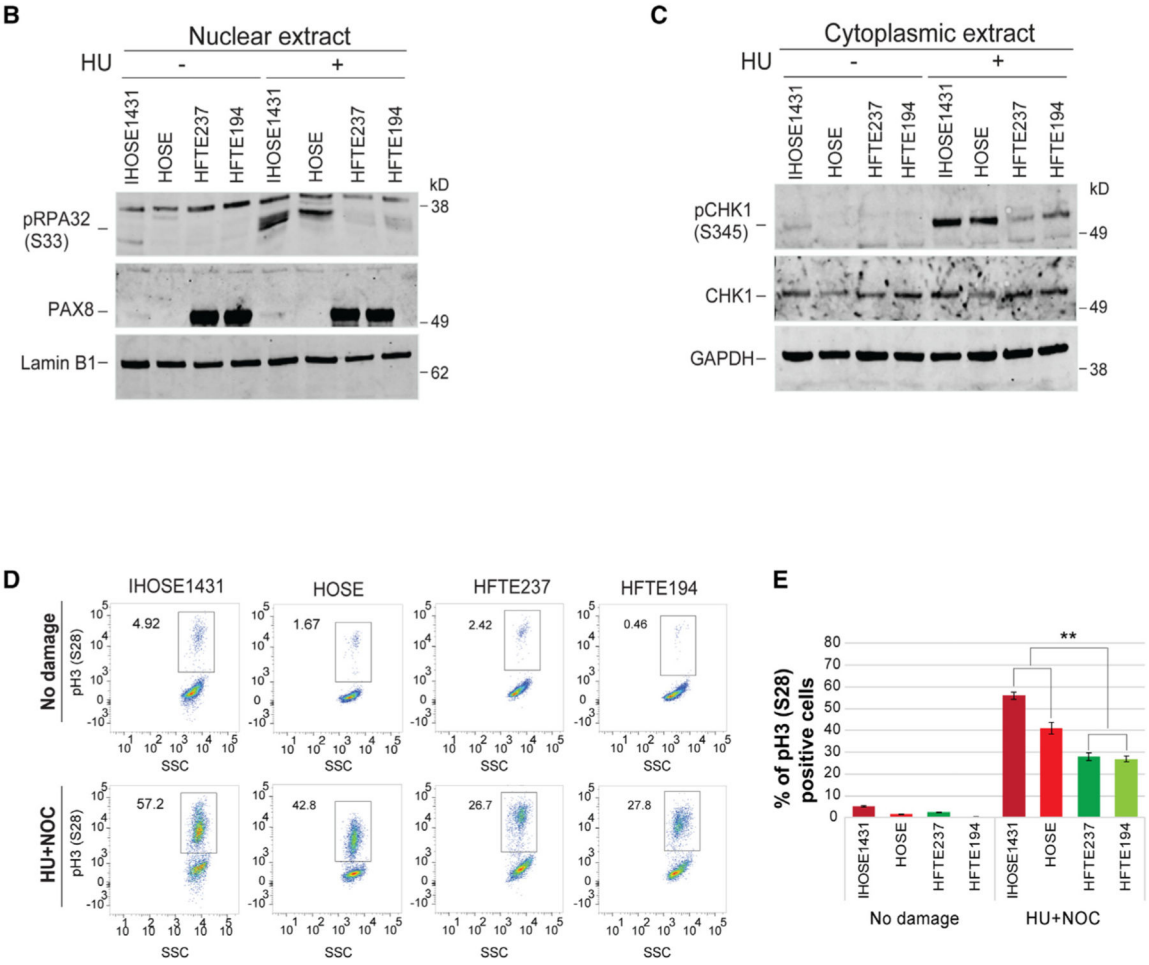

Figure 6. Human fallopian tube epithelial (HFTE) cells are defective in replication-stress suppression and checkpoint activation

(A) List of HOSE and HFTE cell lines used in this study and the genetic modifications each line carries.

(B) pRPA (S33) accumulation in the nuclear extracts of HOSE and HFTE cells. Cells were treated with 5 mM HU for 3 h and the nuclear extract was analyzed by western blot for pRPA (S33), PAX8, and Lamin B1 (loading control).

(C) CHK1 phosphorylation (pCHK1) was analyzed in the cytoplasmic extracts prepared from cells treated with 5 mM HU for 3 h. Western blot was probed for pCHK1 (S345) and CHK1.

(D and E) HOSE and HFTE cells were treated with 2 mM HU for 5 h, and the cells were cultured in medium containing 0.1 μg/mL nocodazole for 18 h. Following 18 h of nocodazole treatment, the cells were collected for FACS-based analysis. (D) Cells were stained with the mitotic marker pH3 (S28) and with propidium iodide (PI). (E) Graph indicates the percentage of pH3 (S28)-positive cells with and without HU and nocodazole treatment. Error bars indicate the SD between two biological replicates. NS indicates not significant; **$p \leq 0.01$.

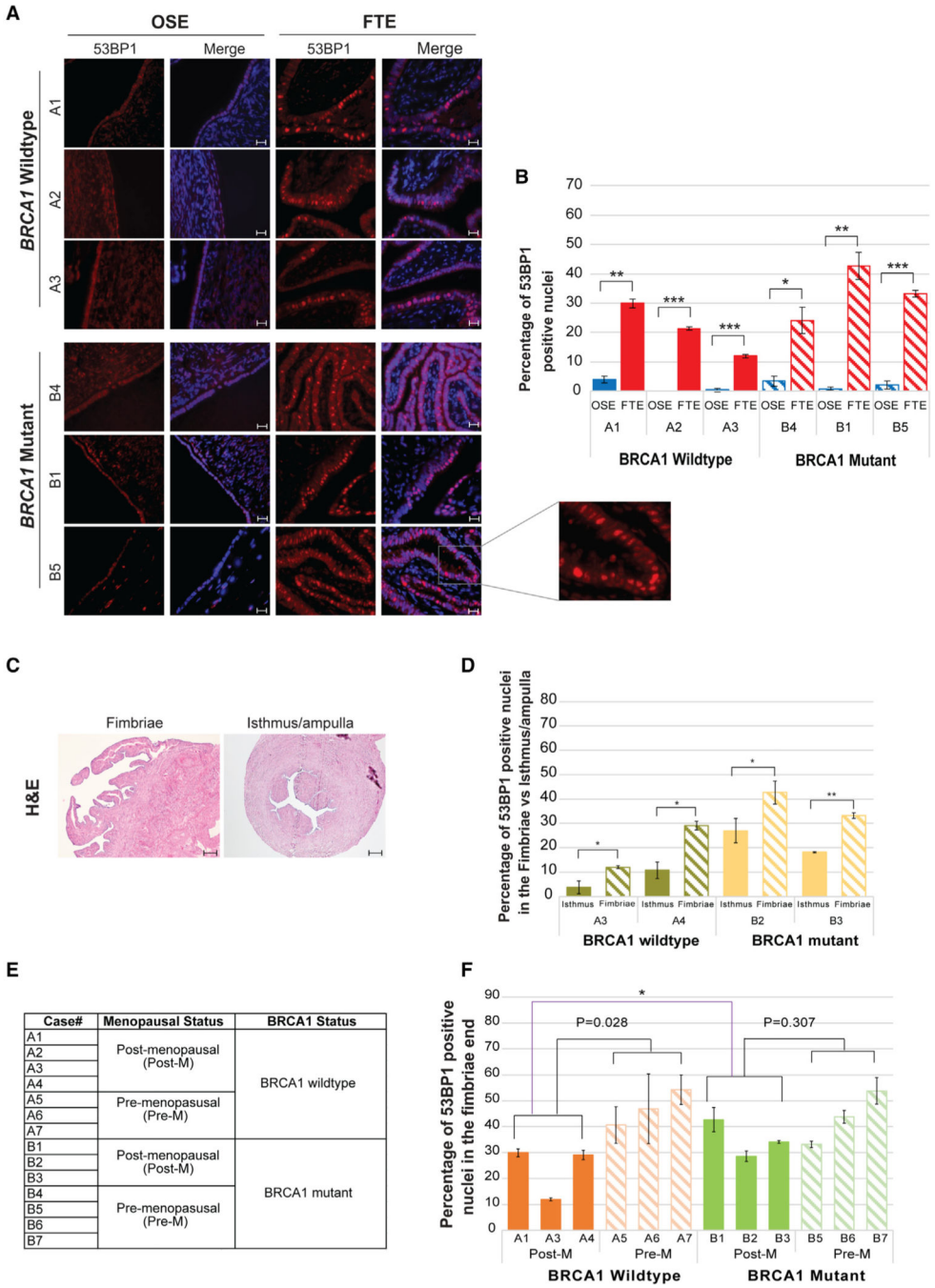

Case#	Menopausal Status	BRCA1 Status
A1	Post-menopausal (Post-M)	BRCA1 wildtype
A2		
A3		
A4		
A5	Pre-menopausal (Pre-M)	
A6		
A7		
B1	Post-menopausal (Post-M)	BRCA1 mutant
B2		
B3		
B4	Pre-menopausal (Pre-M)	
B5		
B6		
B7		

Figure 7. Increased accumulation of replication stress marker 53BP1 in the fallopian tubes and not in the paired ovarian surface epithelium

(A and B) 53BP1 staining in paired fallopian tube and ovarian tissue sections from women with and without *BRCA1* mutation. (A) Representative images of 53BP1 staining in paired ovarian surface epithelium and fallopian tubes of women with and without *BRCA1* mutation. Images were taken at 63× magnification and scale bar represents 20 μm. (B) Percentage of 53BP1-positive nuclei was determined by counting approximately 300 nuclei per section and two sections per case. *p ≤ 0.05, **p ≤ 0.01, and ***p ≤ 0.001.

(C and D) (C) Representative images of H&E staining of fimbriae and isthmus/ampulla region of the fallopian tube. H&E images were taken at 5× magnification. Scale bars represent 200 μm. (D) Graph represents a comparison between 53BP1 staining in the isthmus/ampulla and fimbrial ends of the fallopian tubes. The samples were obtained from both *BRCA1* wild-type and *BRCA1* mutant cases, with each pair of samples (isthmus and fimbrial sections) coming from the same woman. *$p \leq 0.05$ and **$p \leq 0.01$
(E) Table summarizing the menopausal status of *BRCA1* wild-type and *BRCA1* mutation-carrying women whose fallopian tube sections were used for this analysis.
(F) Immunofluorescence analysis of 53BP1 staining in the fimbrial ends of the premenopausal (pre-M) and post-menopausal (post-M) *BRCA1* wild-type and *BRCA1* mutant cases. Approximately 300 nuclei per section were counted from two sections per case (two technical replicates). *$p \leq 0.05$.

KEY RESOURCES TABLE

REAGENT or RESOURCE	SOURCE	IDENTIFIER
Antibodies		
γH2AX	Millipore	Cat# 05-636; RRID: AB_309864
PAX8	Proteintech	Cat# 10336; RRID: AB_2918972
CK8	TROMA-I -DSHB	Cat# AB_531826; RRID: AB_531826
53BP1	Bethyl Labs	Cat# A300-272A; RRID:AB_185520
53BP1	BioLegend	Cat# 933002; RRID:AB_2820202
Foxj1	Millipore Sigma	Cat# HPA005714; RRID:AB_1078902
Rad51	Santa Cruz	Cat# SC-8349; RRID:AB_2253533
pRPA32 (S4/S8)	Bethyl Labs	Cat# A300-245A; RRID:AB_210547
pRPA32 (S33)	Bethyl Labs	Cat# A300-246A; RRID:AB_2180847
pCHK1	Cell signaling	Cat# 2348S; RRID:AB_331212
CHK1	Cell signaling	Cat# 2360S; RRID:AB_2080320
Lamin B1	Cell Signaling	Cat# 12586; RRID:AB_2650517
GAPDH	Santa Cruz	Cat# SC-25778; RRID:AB_10167668
Mouse Brca1	Dr. David Livingston	In this paper
P16	Santa Cruz	Cat# SC-1661; RRID:AB_628067
Ki67	Novusbio	Cat# NB500-170; RRID:AB_10001977
pH3(S28)	BD Biosciences	Cat# 558217; RRID:AB_397065
Anti-BrdU	BD Pharmingen	Cat# 556028; RRID:AB_396304
Rat anti-CldU	Abcam	Cat# Ab6326; RRID:AB_305426
Mouse anti-IdU	BD Biosciences	Cat# 555627; RRID:AB_395993
Alexa Fluor 555 goat anti-rat	Invitrogen	Cat# A21434; RRID:AB_2535855
Alexa Fluor 488 goat anti-mouse	Invitrogen	Cat# A10684; RRID:AB_2534064
Biological samples		
Human Ovarian surface epithelial and Fallopian tube epithelial tissue	This Paper	Brigham and Women's Hospital (BWH)

REAGENT or RESOURCE	SOURCE	IDENTIFIER
Chemicals, peptides, and recombinant proteins		
Citrate buffer pH 6	Millipore-Sigma	Cat# C9999
Cisplatin	Millipore-Sigma	Cat# 232120
Hydroxyurea	Millipore-Sigma	Cat# H8627-1G
Corning Matrigel	Fisher scientific	Cat# CB-40234A
Propidium Iodide	BD Pharmingen	Cat# 550825
Critical commercial assays		
Novolink polymer detection kit	Leica	Cat# RE71401-CE
CellTitter-Glo reagent	Promega	Cat# G7572
Experimental models: Cell lines		
M412, M56, M338, M4	In this paper	N/A
CD-1	(Endsley et al. , 2015)[71]	Dr. Joanna Burdette's Lab
IHOSE1431	(Shin et al. , 2018)[47]	Dr. Jae-hoon Kim's Lab
HOSE	(F et al. , 2007)[46]	Dr. Frances Balkwill's Lab
FTE237	(Karst and Drapkin, 2012)[48]	Dr. Ronny Drapkin's Lab
FTE194	(Perets et al. , 2013)[30]	Dr. Ronny Drapkin's Lab
IHOSE1431ht	In this paper (hTERT immortalized)	N/A
Experimental models: Organisms/strains		
NSG (NOD.Cg-*Prkdc*^{scid}*Il2rg*^{tm1Wjl}/SzJ)- 6weeks old	The Jackson Labs	Cat# 005557
Meox2-Cre mice (Meox2$^{tm1(cre)Sor}$/J)- 14 weeks old	The Jackson Labs	Cat# 003755
Oligonucleotides		
Meox2Crewt: CGCGATTATGCAAGACGAGGAAGATGTGGAGAGTTCGGGGTAG	(Pathania et al. , 2014)[32]	Dr. Pathania's Lab
Meox2CreKI: CTTCTTCTTGGGTCCTCCCAGATCCTCCTCAGAAATCAGC	(Pathania et al. , 2014)[32]	Dr. Pathania's Lab
Meox2Crecommon: CCTGAAAGCAGTTCTCTGGGACCACCTTCTTTTGGCTTC	(Pathania et al. , 2014)[32]	Dr. Pathania's Lab
Brca1-A: GGTACCAGTTATGAGTTAGTCGTGTGCCTGAGTCA	(Pathania et al. , 2014)[32]	Dr. Pathania's Lab

REAGENT or RESOURCE	SOURCE	IDENTIFIER
Brca1-B: GCTGAGATTAAAGTGCAGGCCACCACACTCAGTGAT	(Pathnaia et al. , 2014)[32]	Dr. Pathania's Lab
Brca1-C: GCTGTGACATATTCTTACTTCGTGGCACATCTCTCA	(Pathania et al. , 2014)[32]	Dr. Pathania's Lab
Tp53int1F:ACAAAAAACAGGTTAAACCCAGCTTGACCAAGTGCCATTGGTCCATGGAT	In this paper	N/A
Tp53int1R:AGCACATAGGAGGCAGAGACAGTTGGAGGCCAGCCTGGTCTACAGA	In this paper	N/A
Tp53int10R:GGGGAGGGATGAAGTGATGGGAGCTAGCAGTTTGGGCTTTCCTCCTTGATCA	In this paper	N/A
Recombinant DNA		
PTEN CRISPR/ Cas9 KO plasmid (m)	Santa Cruz Biotechnology	Cat# sc-422475
Software and algorithms		
Graphpad Prism 9.4.1	GraphPad software	https://www.graphpad.com/features
QuPath v0.4.3	QuPath software	https://qupath.github.io/
FlowJo 10.8.1	FlowJo software	www.flowjo.com